(BL2B1)

Development of a New Electron–Ion Coincidence Spectrometer

Kazuhiko Mase, Mitsuru Nagasono, Shin–ichiro Tanaka, and Tsuneo Urisu

Institute for Molecular Science, Okazaki 444–8585, Japan

Energy–selected electron ion coincidence (EICO) spectroscopy is an ideal tool for investigations of the ion desorption induced by electronic transitions, because it provides ion mass spectra for the ion desorption channels related to the selected electron transitions [1]. Recently, we have developed an EICO apparatus combined with synchrotron radiation for the study of surface dynamics at BL2B1 in UVSOR [2]. Auger electron photoion coincidence (AEPICO) spectroscopy demonstrated that the character of the orbitals where holes are created, as well as the effective hole–hole Coulomb repulsion are critical factors which influence ion desorption probability derived from Auger final states [3]. Photoelectron photoion coincidence (PEPICO) spectroscopy, on the other hand, provided direct evidences of site–specific ion fragmentation induced by core–electron excitations [4]. In the present article, we describe details of a remodeled EICO spectrometer developed recently.

The EICO apparatus consists of a cylindrical mirror electron energy analyzer (CMA) and a time–of–flight ion mass spectrometer (TOF–MS) (Figure 1). The solid angle and the resolution of the CMA can be altered by changing the exit slit, that is, $E/\Delta E \geqq 100$ at the solid angle of 0.50 sr, and $E/\Delta E \leqq 80$ at 1.0 sr. The ion collection efficiency of TOF–MS is 40%. The merits of the new apparatus are high resolution, high sensitivity, high signal–to–background ratio, low noise, low cost, and high performance. The data acquisition time is reduced by a factor of 1/5 as compared with that for the first apparatus. The new spectrometer has greatly enhanced the activity of EICO users group at BL2B1 [5].

References

[1] K. Mase *et al.*, *J. Jpn. Soc. Synchrotron Rad. Res.* **10**, 1 (1997) (in Japanese).

[2] K. Mase *et al.*, *Rev. Sci. Inst.* **68**, 1703 (1997).

[3] M. Nagasono *et al.*, *Surf. Sci.* **377–379**, 380 (1997).

[4] S. Nagaoka *et al.*, *J. Chem. Phys.*, **107**, 10751 (1997); Mase *et al.*, *Surf. Sci.* **377–379**, 376 (1997).

[5] K. Mase *et al.*, *Surf. Sci.* **390**, 97 (1997); M. Nagasono *et al.*, *Surf. Sci.* **390**, 102 (1997); T. Sekitani *et al.*, *Surf. Sci.* **390**, 107 (1997); S. Tanaka *et al.*, *Surf. Sci.* **390**, 204 (1997).

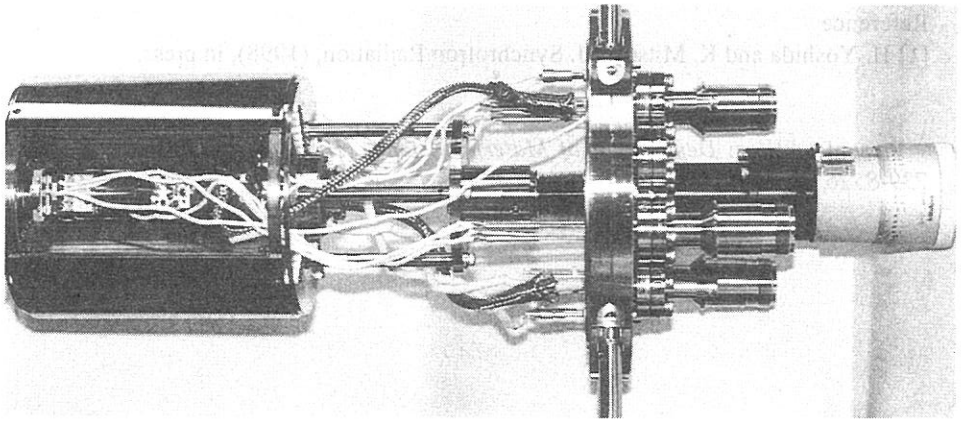

Figure 1. Photograph of the new EICO spectrometer.

(BL2B2) **Construction of an 18m Spherical Grating Monochromator**

Hiroaki YOSHIDA[A] and Koichiro MITSUKE

Department of Vacuum UV Photoscience, Institute for Molecular Science, Myodaiji, Okazaki 444-8585, Japan

An 18 m spherical grating monochromator (18 m SGM) with high resolution and high photon flux has been developed at the bending-magnet beamline BL2B2 of the UVSOR[1]. The monochromator is designed to cover the energy range of 20-200 eV. A resolving power of 5000 and photon flux of more than 10^{10} photons s^{-1} are expected at a 100 mA ring current. A small including angle of 140° is adopted for G3 and two plane mirrors coated with aluminium are located between G3 and the exit slit as optical filters. These geometrical devices may contribute significantly to reduction of the high-order lights.

A schematic layout of the beamline is shown in Fig. 1. The optical system consists of two prefocussing mirrors (M0 and M1), a fixed entrance slit (S1), an aperture (AP), a spherical grating (G1, G2 or G3), two folding mirrors (M2 and M3), a movable exit slit (S2) and a refocussing mirror (M4). The first mirror M0, which is located 2.136 m downstream from the source point in the electron storage ring, deflects the photon beam by 13°. Vertical and horizontal acceptance angles of this mirror are 6 and 15 mrad, respectively. It serves as a horizontal focussing mirror with a focal distance of 7 m. This mirror is installed in the same vacuum chamber as a prefocussing mirror of the neighboring beamline BL2B1. Spatial restriction imposed from the beamline BL2B1 determines the axis of our monochromator. The vertical prefocussing mirror M1 is placed 1.8 m behind M0 with a demagnification of 3:1 and a grazing angle of 5°. To decrease distortion induced by heat load, M0 and M1 are equipped with water-cooling systems.

The monochromator is designed to cover the energy range of 20-200 eV with the three gratings: G1 (2400 lines mm^{-1}, R = 18 m) at 80-200 eV , G2 (1200 lines mm^{-1}, R = 18 m) at 40-100 eV and G3 (2400 lines mm^{-1}, R = 9.25 m) at 20-50 eV. The including angles are 160° for G1 and G2 and 140° for G3. The directions of the incident and exit photon beams are fixed. The arm length of S1 from the grating is fixed at 2 m, while that of S2 varies from 4.18 to 4.58 m. A wavelength scanning mechanism is very simple because movement of the grating is confined only to mechanical rotation. A set of optical filters, i.e., the plane mirrors M2 and M3, are inserted across the photon beam between G3 and S2, which may significantly reduce the high-order lights of G3. These mirrors can be removed from the optical path without breaking vacuum when G1 or G2 is chosen. The coma aberration of spherical gratings is expected to be greatly decreased by AP placed 1 m from S1.

The refocussing mirror M4 is located 1.46 m downstream from the mean position of S2, deflecting the photon beam by 10° to make it horizontal. Demagnifications of vertical and horizontal directions are 1:1 and 2.75:1, respectively. The distance from the source point to the sample point is about 14.7 m.

Parameters of the optical elements are summarized in Table 1. The M0 mirror is fabricated by Hidaka Kougaku Kenkyusyo Inc. (Japan) and the other mirrors by Optron Inc. (Japan). All the optical elements are made of quartz coated with Au except M2 and M3 which are coated with Al to substantially prevent the reflection of the high-order lights. Ion-etched holographic laminar gratings are manufactured by JOBIN-YVON, Div. of INSTRUMENTS S. A. (France). Slope errors of G1, G2 and G3 are 0.28, 0.25 and 0.18 arc sec, respectively.

This monochromator was manufactured by TOYAMA Co., Ltd. (Japan) and assembled at UVSOR in May 1997. At present the optical alignment is being performed.

The authors would like to gratefully acknowledge useful suggestions from Professor Atsunari Hiraya of Hiroshima University, Professor Akira Yagishita of Photon Factory, Dr. Yonglian Yan of BSRL in China and Professor Eiji Ishiguro of Ryukyu University.

Reference

[1] H. Yoshida and K. Mitsuke, J. Synchrotron Radiation, (1998), in press.

[A] Present address: *Department of Material Science, Hiroshima University, Kagamiyama, Higashi-Hiroshima 739-8526, Japan*

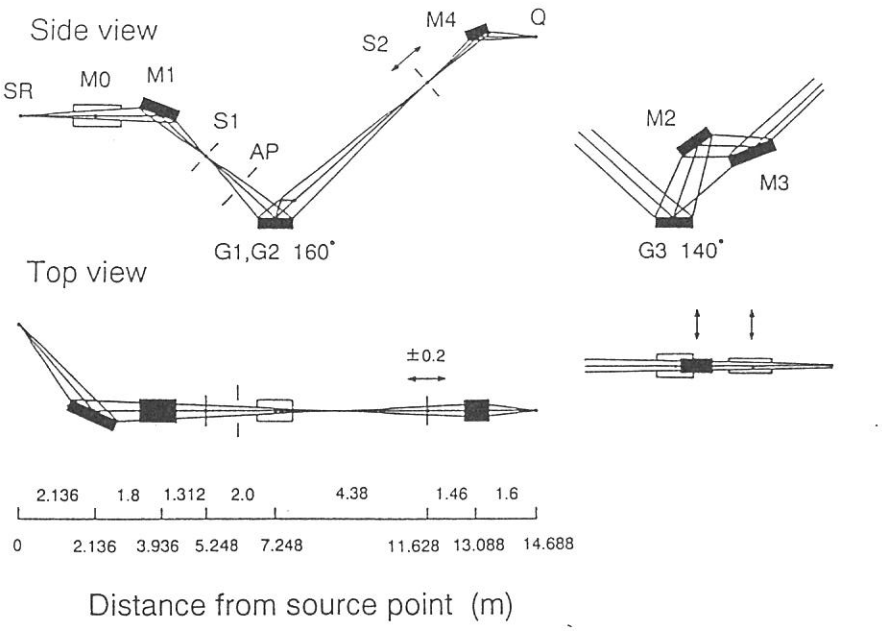

Fig. 1 Schematic layout of renewed BL2B2 equipped with an 18 m SGM. Two optical paths with including angles of 160° for G1 and G2 and 140° for G3 are indicated. SR, synchrotron radiation source point; M0, elliptically bent plane mirror; M1, spherical mirror; S1, entrance slit; AP, aperture; G1, G2 and G3, spherical gratings; M2 and M3, plane mirrors; S2, exit slit; M4, toroidal mirror; Q, sample point.

Table 1 Parameters of mirrors and gratings of 18 m SGM

Mirror	M0	M1	M2	M3	M4
Shape	Elliptical [a]	Spherical	Plane	Plane	Toroidal
Radii R× ρ (mm) [b]	28914 [c]	23405			18341×202.2
Material	quartz	quartz	quartz	quartz	quartz
Coating (nm)	Au 100	Au 100	Al 100	Al 100	Au 100
Reflective area L×W (mm)	500×20	400×34	250×24	600×24	300×50
Micro roughness (Å rms)	—	3.29	3.08	1.42	5.0
Grazing angle (°)	6.5	5.0	15.0	5.0	5.0

Grating	G1	G2	G3
Shape	Spherical	Spherical	Spherical
Radius (mm)	17987±18	17987±18	9246±6
Groove density (lines mm^{-1})	2400	1200	2400
Duty ratio [d]	0.61	0.675	0.62
Groove depth (nm)	11.4	22.6	23.5
Au coating (nm)	40±4	40±4	40±4
Material	quartz	quartz	quartz
Ruled area L×W (mm)	130×20	130×20	130×20
Size L×W×t (mm)	140×30×25	140×30×25	140×30×25
Micro roughness (Å rms)	3.6	< 5	< 5
Slope error (arc sec)	< 0.28	0.25	0.18
Including angle (°)	160	160	140

[a] Elliptically bent plane mirror.
[b] Tangential (R)×sagittal (ρ).
[c] Radius at the center of the mirror.
[d] Groove width / pitch.

(BL2B2, 3A2)

Construction and Apparatus of the Two-Dimensional Photoelectron Spectrometer at Beamlines 2B2 and 3A2

Koichiro Mitsuke[A], Kota Iwasaki[A,B], Hiromichi Niikura[A,C]
Masakazu Mizutani[A], and Yasumasa Hikosaka[A]

[A] *Institute for Molecular Science, Myodaiji, Okazaki 444-8585, Japan*
[B] *Inoue Fellow; Inoue foundation for Science, Sarugaku-cho, Shibuya-ku, Tokyo 150, Japan*
[C] *The Graduate University for Advanced Studies*

Vacuum UV photoexcitation of an electronically-ground-state molecule induces various phenomena, *i.e.* direct ionization, shape resonance, superexcitation, autoionization, direct dissociation, predissociation, fluorescence emission, nonradiative transition (nonadiabatic transition, internal conversion and intersystem crossing, *etc.*), and binary or trinary combinations of these processes. As a rule, electron emission due to direct ionization or autoionization dominates over the other processes, even if the energy transferred to the molecule is not more than few electron volts above its first ionization potential. Hence, photoelectron spectroscopy is considered to be crucially helpful in our understanding the mechanism of VUV photoexcitation and subsequent decay channels of gas-phase molecules as well as condensed matters.

In UVSOR, beamline 3B is devoted to the gas phase two-dimensional photoelectron spectroscopy. Here, the term "two-dimensional" means that photoelectron yield is measured as a function of both photon energy and electron kinetic energy (binding energy). A two-dimensional spectrum, usually represented as a contour plot, contains rich information on photoionization dynamics and properties of superexcited states (see the *Current status of beamline 3B* in this journal). Unfortunately, a wavelength or photon-energy coverage of our normal incidence monochromator connected with BL3B ranges from 35 to 200 nm or from 6 to 35 eV, respectively, so that feasible subjects are limited to elementary atomic and molecular processes caused by outer-valence-electron excitation. To extend our knowledge over the research fields of inner-valence- and inner-shell-electron excitations, we should carry out photoelectron spectroscopy at beamlines equipped with a grazing-incidence monochromator. UVSOR facility has a few beamlines for gaseous experiments which can supply photons of higher energies than BL3B. In the present report, description is made on construction of a new apparatus of two-dimensional photoelectron spectroscopy which is now set downstream of a constant-deviation grazing-incidence monochromator at the undulator beamline 3A2. Furthermore, this apparatus is scheduled to be incorporated into a performance test system for a new Dragon-type monochromator which is under construction at the bending-magnet beamline 2B2. The former monochromator is designed to cover the energy range from 13 to 120 eV, while the latter from 20 to 200 eV.

Figure 1 shows a schematic diagram of a measurement chamber which contains an electron energy analyzer of 166° spherical electrostatic deflection type, a quadrupole mass spectrometer, a detector of photon pulses, and a gold-mesh current monitor. The energy dispersed electrons are detected with a position sensitive detector (PSD) composed of dual microchannel plate (MCP) multipliers and a two-dimensional resistive-anode encoder. Detection efficiency of PSD is expected to be about 50 times as high as that of a single channel MCP detector, as far as other conditions are the same, since PSD can collect all of the energy-dispersed electrons simultaneously that can pass through between the two spherical sector surfaces. The kinetic energy can be precisely determined from a displacement of the location of the incident electron along the

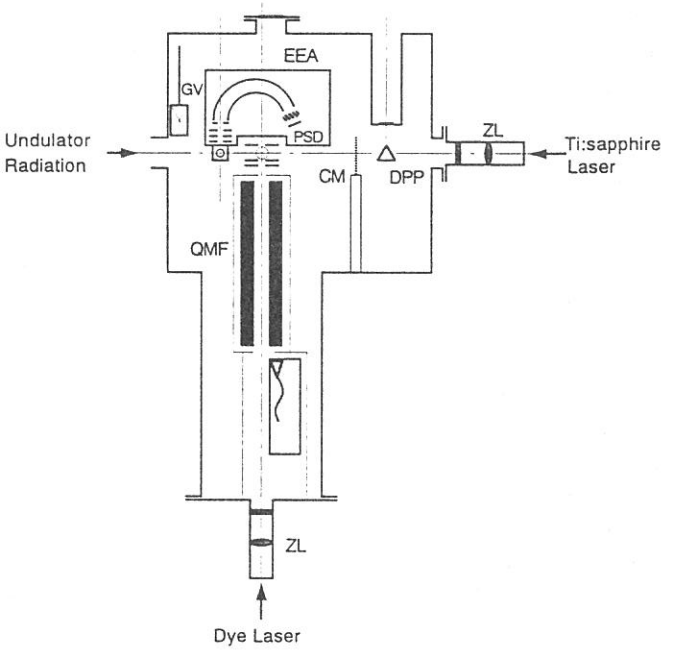

Figure 1. Schematic diagram of the apparatus. GV, gate valve; QMF, quadrupole mass filter; EEA, electron energy analyzer; PSD, position sensitive detector; CM, gold-mesh current monitor; DPP, detector of photon pulses; ZL, zoom lens.

coordinate of energy dispersion. Measuring two-dimensional photoelectron spectra are controlled by the CAMAC and NIM systems. Figure 2 shows a dependence of the energy resolution ΔE (FWHM) on the transmission energy T_E of electrons traveling inside the analyzer. Open circles represent experimental peak widths determined from the $Ar^+(^2P_{3/2}, {}^2P_{1/2})$ bands in photoelectron spectra of Ar taken by using the He I resonance line (photon energy of 21.218 eV) furnished from a supplementary helium discharge lamp. The solid line shows a plot of theoretical band widths (FWHM) estimated by assuming both the entrance and exit slits of 4 mm diameter. At T_E higher than 2 eV, every experimental ΔE value is smaller than obtained by theoretically, since the present PSD has a spatial resolution of 250 μm. On the other hand, ΔE values at T_E lower than 1 eV appear to be about twice as large in the experiment as in the theory. This lowering of the resolving power is probably ascribed to a remaining magnetic field in a part of PSD, which will soon be replaced. Figure 3 shows a photoelectron spectrum of O_2 containing a little amount of Ar measured by using the undulator radiation from BL3A2. The photon energy and overall energy resolution are set to 23.934 and 0.07 eV, respectively.

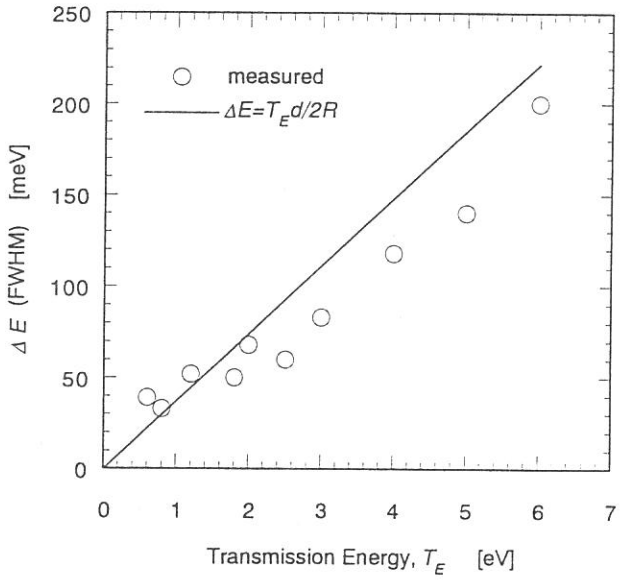

Figure 2. Dependence of the energy resolution ΔE (FWHM) on the transmission energy T_E. In the theoretical equation, d and R denote the width of entrance and exit slits and the mean radius of the electron orbit.

The instrument illustrated in Fig. 1 has been especially designed and fabricated toward another important final goal, that is two-photon ionization photoelectron spectroscopy using time-correlated synchrotron radiation and laser photon pulses. For this purpose, a laser beam can be introduced through a zoom lens unit so as to counterpropagate the synchrotron radiation beam. Synchronization of the laser to synchrotron radiation is performed by use of an electronics module which provides phase-locked stabilization of laser pulses. The temporal overlap of the two photon pulses can be adjusted by monitoring the signal from the detector of photon pulses. In addition, we are planning to fulfill resonance-enhanced-multiphoton ionization (REMPI) spectroscopy of dark neutral fragments produced by competitive (pre)dissociation of superexcited states.

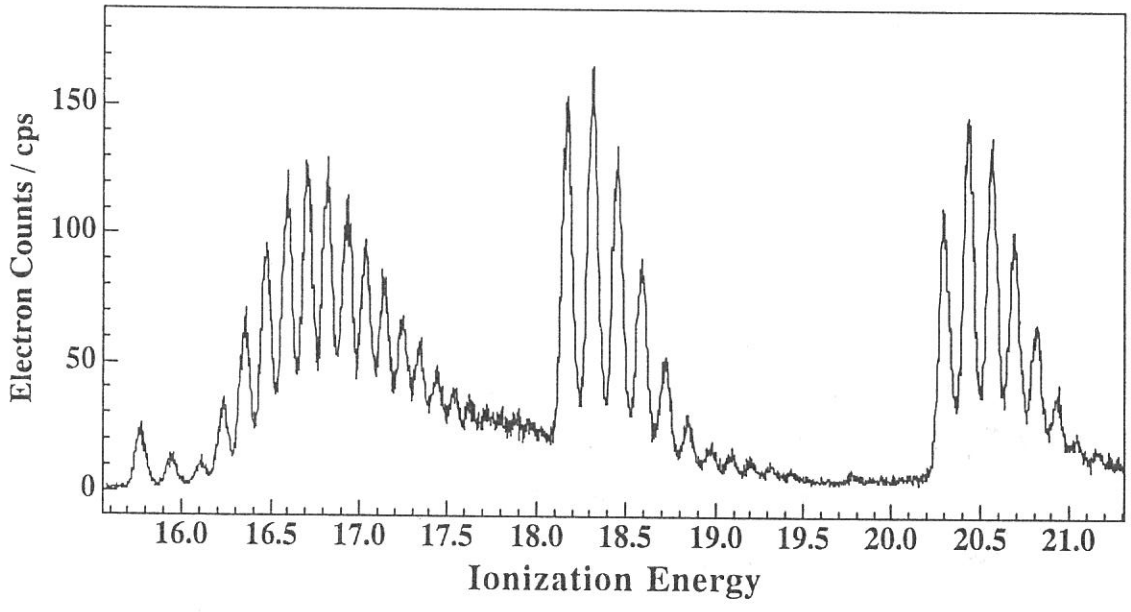

Figure 3. Photoelectron spectrum of O_2 containing a little amount of Ar measured by using the undulator radiation from BL3A2. The photon energy and overall energy resolution are set to 23.934 and 0.07 eV, respectively.

(BL3A2)

Two-dimensional imaging technique for measuring translational energy and angular distribution of ionic photofragments

Tatsuo GEJO and Norio SAITO [A]

Institute for Molecular Science, Myodaiji, Okazaki 444-8585, Japan

[A] *Electrotechnical Laboratory, Umezono, Tsukuba-shi, 305-0045, Japan*

The dynamics of molecular in the valence energy regime can be investigated by preparing to excited state at well-defined energy and analyzing the ionic photofragments. Two dimensional imaging technique is one of the most powerful methods for obtaining this information because calculation on the basis of momentum conservation law provides Newton diagram of photofragments. We have launched the two dimensional imaging technique with using a position sensitive detector (PSD) at BL3A2 in UVSOR.

The machine consists of a beam nozzle, a skimmer, ion lenses, an position sensitive detector with MCP (fig. 1). This configuration is particularly suitable for PIPICO and PIPIPICO technique because symmetric configuration of ion lens and MCP around the molecular beam axis minimize the affect of the initial velocity distribution of the beam. After being skimmed, the molecular beam pass thorough SR region, and less than one molecular per one photon beam on the average undergo ionization and/or dissociation. Accordingly it allows an coincidence technique. After the acceleration by ion lens, ion fragments hit the PSD. The determination of position on the detector is based on the time delay between two signals from each end of an wire behind the MCP: The position is obtained by the subtracting of time when each two signals arrive. Since the direction of polarization of SR is parallel to the axis of TOF tube, the TOF and the position of the ionic fragments on the detector provide its velocity and direction in center-of-mass frame.

At BL3A2 we have successfully measured the image of N^+ and N_2^+ signal from nitrogen at the valence region (20-100 eV). However, significant noise level excluded us from analyzing the data. This noise mainly comes from the fluctuation of the ground level caused by RF signals at the storage ring. The improvement of the detection system will allow us to obtain the data.

We thank Prof. T. Suzuki at IMS for his technical advice.

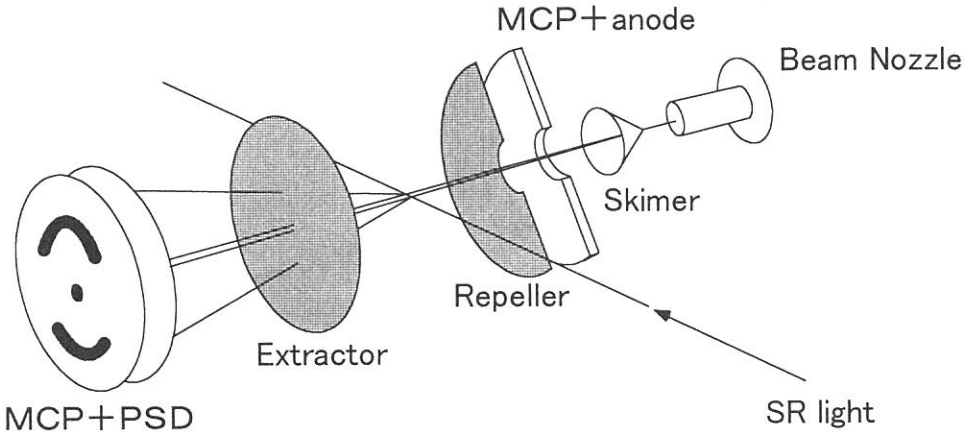

Fig. 1: Schematic view of 2D imaging technique

(BL4A1)

Performance of the Double Multi-Layered-Mirror Monochromator and Beamline BL-4A1

Harutaka Mekaru[A],Takayuki Miyamae[B] and Tsuneo Urisu[B]

[A]The Graduate University for Advanced Studies,
[B]Institute for Molecular Science, Myodaiji, Okazaki 444-8585

The authors developed a double multilayered mirror (MLM) monochromator and constructed the beamline BL-4A1 at the UVSOR for studies of synchrotron radiation (SR) stimulated processes.

The important photon energy region for the experimental investigation of SR stimulated processes, especially of the core electron excitation processes, is from a few tens to hundreds of electron volts. In the present work, our attention was focused on the region between 60 and 120 eV that includes the core electron binding energy of Al (2s : 119eV, 2p : 74eV) and Si (2p : 103eV). In this region a fairly high reflectivity is obtained by using Mo/Si (for 60-120eV) and Mo/C (for 85-120eV) MLMs. Further, a carbon 100nm thick filter was combined to remove the background noise of the low energy region consisting of total reflection components

In this report we present experimental results for the performance of a double MLM monochromator in the energy range 60 to 128eV and compared to calculations. Measurements of the Al $L_{2,3}$ (72eV) absorption edge using Mo/Si MLMs with a C filter and the Be K (111.5eV) absorption edge using Mo/C MLMs with a C filter are also presented and compared with calculations. The photon flux was estimated between 2×10^{13} and 8×10^{15} photons/cm^2. The energy selectivity of the MLM monochromator and Al $L_{2,3}$ edge and Be K edge are clearly seen. The measured maximum transmission of the monochromator using Mo/Si MLMs is 42% with a resolution of ΔE=6.4eV and that using Mo/C MLMs is 13% with a resolution of ΔE=5.6eV. We conclude that the photon flux and the resolution are sufficient performance for studies of SR stimulated processes.

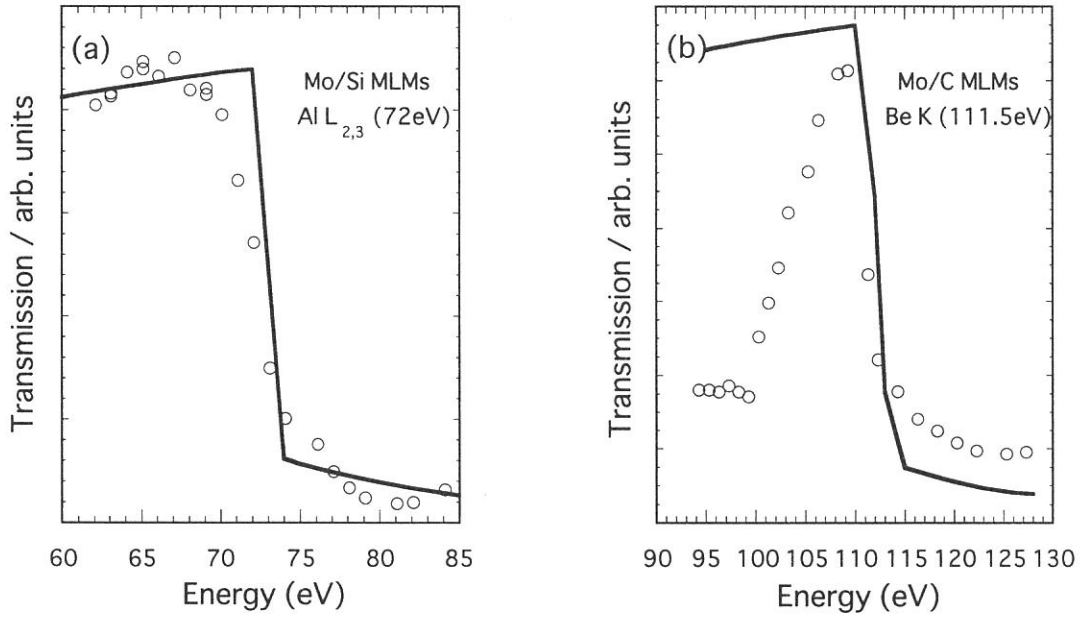

Figure 1 Transmission of the 120 nm thick aluminum filter measured (dots) and calculated (solid line) in the vicinity of the Al $L_{2,3}$ edge using Mo/Si MLMs (a) and the 100nm thick beryllium filter measured and calculated in the vicinity of the Be K edge using Mo/C MLMs (b).

(BL4B)

Development of UHV-STM System for Study of Surface Photochemical Reactions Induced by Synchrotron Radiation.

Takayuki MIYAMAE[a], Shinya HIRANO[b], Hironaga UCHIDA[c], and Tsuneo URISU[a]

[a] *Institute for Molecular Science, Myodaiji, Okazaki 444-8585*

[b] *The Graduate University for Advanced Studies*

[c] *Toyohashi University of Technology, Toyohashi 441*

We have newly developed a scanning tunneling microscopy (STM) system for the study of surface photochemical reactions. The design of our UHV-STM system is schematically shown in Fig. 1. The STM is located in the left-hand side of the main chamber. A back-view LEED, an atomic hydrogen doser, and a heating device are located on the right-hand side of the chamber. The pumping of the system is carried out by ion pump, Ti sublimation pump, and a non-evapolable getter pump for the main chamber and a turbomolecular pump for the sample preparation chamber which is stopped during the STM experiments. A pressure better than 1×10^{-10} Torr can be maintained in the main chamber. The STM body is suspended by three stainless steel springs for vibration isolation. The entire UHV system is mounted on an air-suspended vibration isolation table. STM images of the Si(111)-7×7 clean surface and atomic hydrogen-chemisorbed surface are shown in Fig. 2. Now experiments using STM for the geometrical topography and electronic structure of atomic hydrogen-chemisorbed Si surface and its change by the synchrotron radiation stimulated surface reaction is underway.

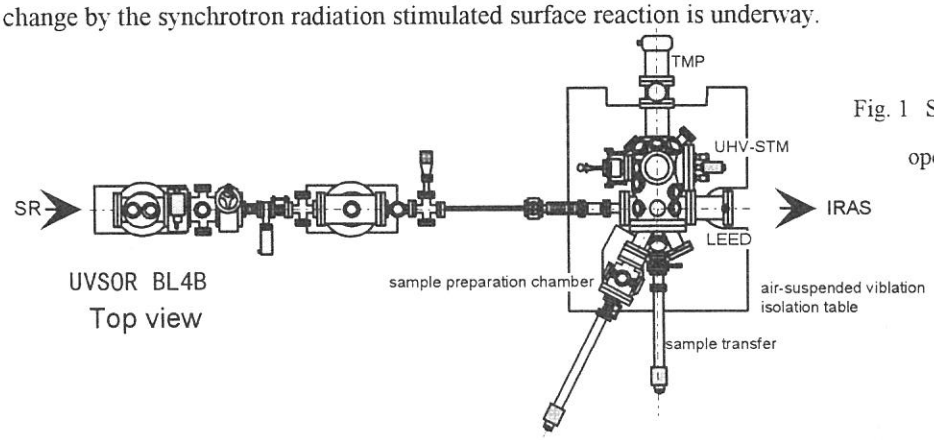

Fig. 1 Schematic of the STM system operated in the UHV condition.

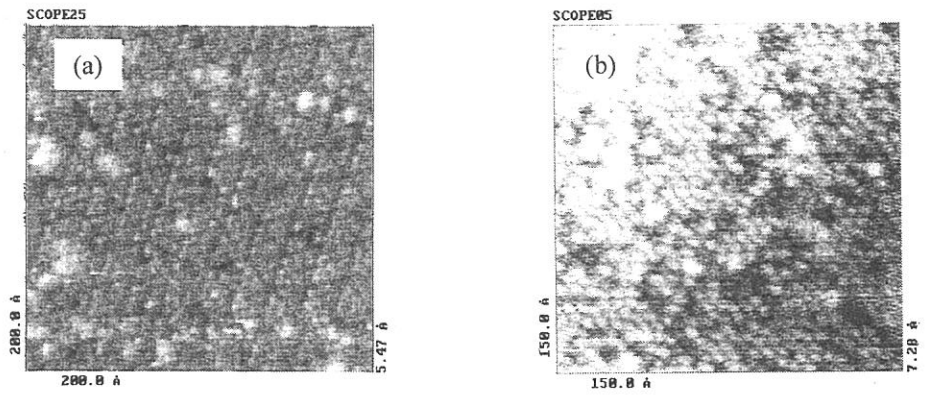

Fig. 2 STM images of the occupied states of the Si(111) clean surface (a) and the surface following a low coverage exposure to H atoms (b).

(BL5A)

Performance of the electron spectrometer for the high-resolution photoelectron spectroscopy at BL5A

Shin-ichiro Tanaka, Jun-ichi Murakami and Masao Kamada

Institute for Molecular Science, Okazaki, 444-8585, Japan

BL5A is consists of a helical undulator, an SGM-Train (Spherical Grating Monochromator with Transnational and Rotational Assemblies Including Normal-incidence mount) monochromator and a UHV chamber which equipped with a LEED optics, a CMA (cylindrical Mirror Analyzer) for the Auger electron spectroscopy, an ion gun, a gas-dose system using a pulse valve, a spin- and angle- resolved electron spectrometer, a hemispherical electron analyzer for high resolution photoelectron spectroscopy and a sample holder with a liquid-He cryostat. In this report, we describe the hemispherical analyzer and the sample holder, and show an achieved performance.

The hemispherical analyzer is "EA-125HR" made by OMICRON, Germany, which consists of the 11-element zoom lens, a 180° hemispherical analyzer of 125 mm mean radius and a detection system with 5 channeltrons. The potential of lens (selectable among 3 magnification modes) is controlled by the PC (Gateway 2000) via the "EAC-300" control unit. The data detected with 5 channeltrons are shifted in energy and added to make one spectrum with high count rate. Unfortunately, the simultaneous control of the SGM-Train monochromator and the electron analyzer can not be made yet.

A sample can be cooled by a home-made liquid-He cryostat of a transfer type. The sample is electrically isolated by a sapphire sheet of 1mm thick, and can be heated to more than 1500 K by resistive heating or electronic bombardment from the rear. The sapphire sheet also works as a thermal switch because its thermal resistance varies drastically depending on the temperature. It has a Chromel-Almel thermocouple, but not precisely calibrated at low temperatures. The lowest temperature was estimated by the adsorption and desorption measurements of gases, e.g., CO, O_2, N_2, Ar on the sample, and was less than 25 K.

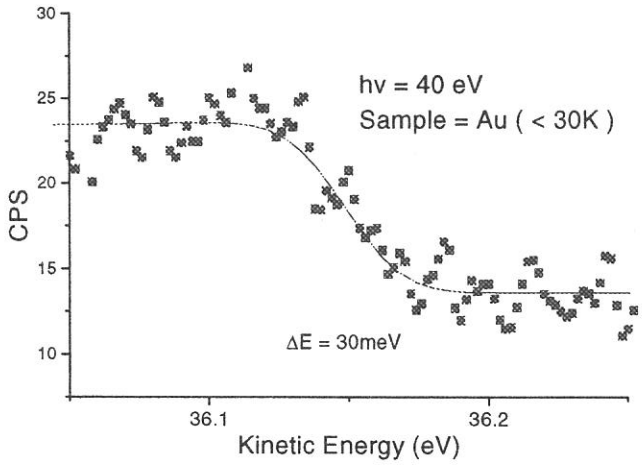

Left figure shows an example of the photoelectron spectrum at the Fermi edge of the Au film measured at BL5A. The photon energy was 40 eV. It is noted that the photon from the bending magnet was used. Solid line is an error function fitted to the data. The ΔE (2σ) in the error function is 30 meV, which includes the Fermi-Dirac distribution, and the instrumental resolution should be better.

(BL5A)

Construction and performance test of SGM-TRAIN at UVSOR

Masao Kamada, Masami Hasumoto, Nobuo Mizutani, Toshio Horigome, Shin-ichi Kimura, Shin-ichiro Tanaka, Kusuo Sakai, and Kazutoshi Fukui*

Institute for Molecular Science, Okazaki 444-8585, Japan
**Fukui University, Fukui 910, Japan*

A new monochromator called SGM-TRAIN (Spherical Grating Monochromator with Translational and Rotational Assembly Including a Normal incidence mount) has been constructed at BL5A. The SGM-TRAIN is designed for experiments where the circularly polarized synchrotron radiation from a helical undulator is used, as well as bending magnet radiation. The SGM-TRAIN has the advantage that the small emittance of a storage ring and the large space for a long beam line are not necessary. The design of the SGM-TRAIN is based on the following requirements: (1) Fundamentals from the helical undulator appear in the photon energy range of 5-43 eV, with the harmonic radiation being emitted up to 250 eV. (2) A floor space limits a distance between the first pre-mirror and a sample position to 8 m. (3) Degree of circular polarization should be kept as high as possible. (4) Higher order light must be suppressed. (5) Bending magnet radiation is used as well as undulator radiation. (6) Beam size and emittance in the vertical direction are 0.52 mm and 11.5 πnm rad, respectively.

The SGM-TRAIN is an advanced version of a constant-length monochromator proposed by Ishiguro et al. (1). The SGM-TRAIN consists of two glancing incidence mounts and a normal incidence mount. The parameters of main optical elements are given in Table I. Pre-mirrors, BM0 and UM0, are used for bending magnet radiation and undulator radiation, respectively. Two post-mirrors, M31 and M32, are exchanged for normal and glancing incidence mounts, and the focus point is about 1.5 m from the post-mirror. Two types of scanning modes, the combination mode of rotation and translation and the rotational mode at fixed translational position, are available in the SGM-TRAIN, since all driving systems are directly controlled by a computer.

Figure 1 shows the doubly ionization spectrum of He at the pressure of 50 mTorr. The spectrum was obtained in the combination scanning mode with 10 μm slits and G2M22. Rydberg lines up to n=11 are clearly observed, indicating a resolving power of about 4,000 at 200 Å. The resolving power of about 3,500 was also obtained from the Ar $L_{2,3}$ spectrum at 50 Å with the combination G1M21. These values are by 20-30 % less than the expected values (2). Figure 2 shows photoelectric yield spectra of a gold mesh for bending magnet radiation. The spectra #1-#4 correspond to the combinations of G1M21, G2M22, G2M23, and G2M24, respectively. Laminar-profiles of the gratings and coating

Table I. Parameters of main optical elements

name	shape	coating	angle(°)	radius(m)	dimension(mm³)
BM0	Toroidal	Au	172	58.540 (ρ = 0.527)	310x25x25
UM0	Spherical	Au	174	181.607	340x25x25
M1	Spherical	Au	175	61.240	420x35x30
M21	Plane	Au	172		110x30x20
M22	Plane	Au	152		60x30x10
M23	Plane	SiC	152		60x30x10
M24	Plane	Al	152		60x30x10
M25	Plane	Pt	7		40x30x10
G1	Spherical	Au	172	25.406	110x30x20
G2	Spherical	Au	152	7.245	60x30x20
G3	Spherical	Au	7	2.549	40x30x20
M31	Toroidal	Au	175	26.090 (ρ = 0.164)	280x30x25
M32	Toroidal	Au	175	28.090 (ρ = 0.079)	280x30x25

materials (Au, SiC, Al, and Pt) on the plane mirrors were chosen in order to suppress the second-order light with less decrease in the degree of circular polarization. Further testing and tuning of the SGM-TRAIN are requested in order to get better performance with circularly polarized light from the helical undulator, which was installed into the one of the straight sections of the UVSOR storage ring .

References

(1) Ishiguro, E, Suzui, M, Yamazaki, J, Nakamura, E, Sakai, K, Matsudo, O, Mizutani, N, Fukui, K, Watanabe, M (1989), Rev. Sci. Instrum. 60, 2105-2110.

(2) Kamada, M, Saka, K, Tanaka, S, Ohara, S, Kimura, S, Hiraya, A, Hasumoto, M, Nakagawa, K, Ichikawa, K, Soda, K, Fukui, K, Fujii, Y, and Ishiguro, E (1995), Rev. Sci. Instrum. 66, 1537-1539.

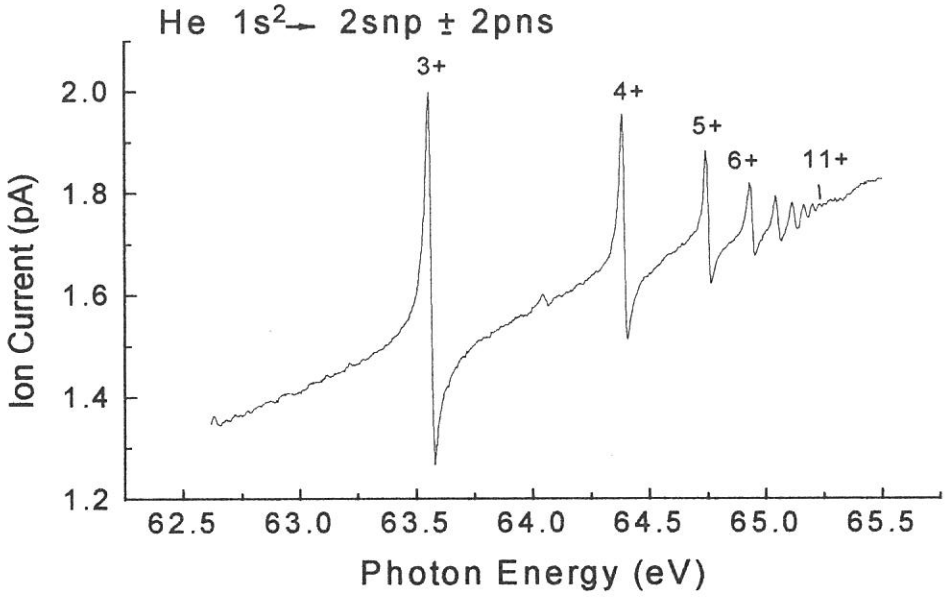

Fig. 1. The doubly ionization spectrum of He at the pressure of 50 mTorr.

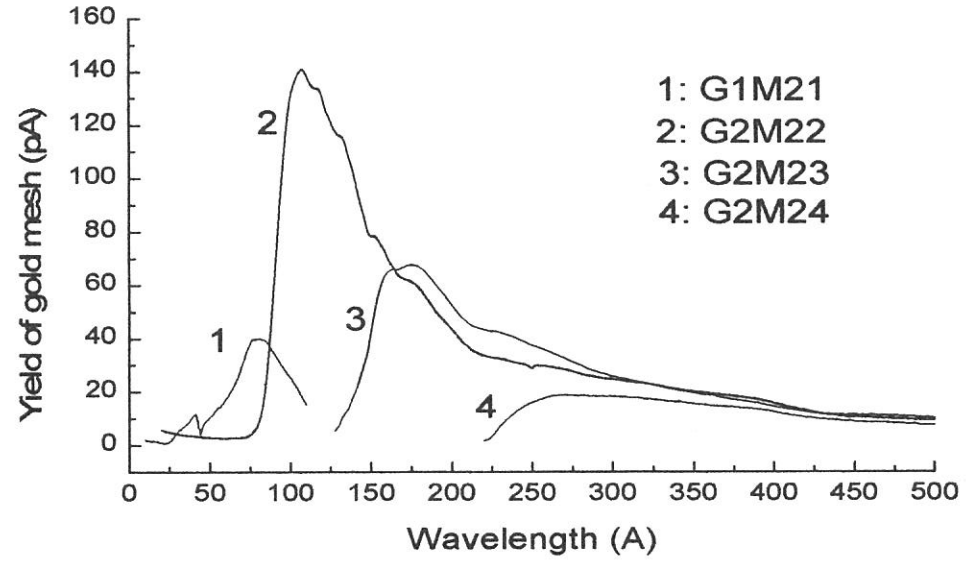

Fig. 2. Photoelectric yield spectra of a gold mesh for bending magnet radiation.

(BL5A)

Performance of The Helical Undulator of BL5A

S. Kimura, M. Kamada, H. Hama, K. Kimura[1], M. Hosaka, J. Yamazaki, X Marechal[2], T. Tanaka[2] and H. Kitamura[2]

UVSOR Facility, Institute for Molecular Science, Okazaki 444-8585
[1]Department of Structural Molecular Science, The Graduate University for Advanced Studies, Okazaki 444-8585
[2]SPring-8, Kamigori, Hyogo 678-12

Optical excitations with circularly polarized light are useful to know magnetic moments of electrons. The difference spectrum between absorption for right and left circularly polarized light is called circular dichroism (CD). The CD method is one of powerful tools for the investigation of electronic structures, not only of magnetic materials but also of non-magnetic materials. On the other hand, a spin-resolved photoelectron spectroscopy can give us information about momentum and spin of electrons. The combination of the circularly polarized light and the spin-resolved photoelectron analyzer allows us to observe the electronic structures of materials with selected magnetic moments.

For the investigation of electronic structures of magnetic and non-magnetic materials by a spin-resolved photoelectron spectroscopy, we have constructed a beam line, BL5A, of UVSOR. The beam line consists of a helical undulator, a high-resolution monochromator and a spin- and angle-resolved photoelectron analyzer. The monochromator, which is named SGM-TRAIN (spherical grating monochromator with translational and rotational assembly including a normal incidence mount), is an improved version of a constant deviation and constant length monochromator [1]. The spin- and angle-resolved photoelectron analyzer is a type of low-energy diffuse scattering [2]. These apparatus have already been completed and reported in elsewhere. Recently, the first spectrum of circularly polarized light in the vacuum-ultraviolet region from the helical undulator was observed. In this paper, the performance of the helical undulator and the observed spectrum are reported.

The UVSOR helical undulator is a modified version of a helical undulator, or an elliptical wiggler [3] and an 8-figure undulator [4] which were designed for the 8-GeV storage ring, SPring-8. Since the energy of UVSOR is about one order less than that of SPring-8, special cares were taken to optimize the magnetic fields. The peak energy of the fundamental radiation can be swept only by changing the undulator gap while keeping the degree of the circular polarization.

The helical undulator has three lanes in the upper and the lower magnet arrays shown in Fig. 1. The undulator looks like a planar one. However, in the helical configuration, the center lane produces the vertical magnetic field and the side lanes make the horizontal field. The vertical and horizontal magnetic fields were set to be almost equal to each other in the undulator gap of 30 – 150 mm. In the range of the undulator gap, the range of the deflection parameter, K, is 4.6 – 0.07. The fundamental emission peak is expected to cover the photon energy range of 2 – 43 eV [5].

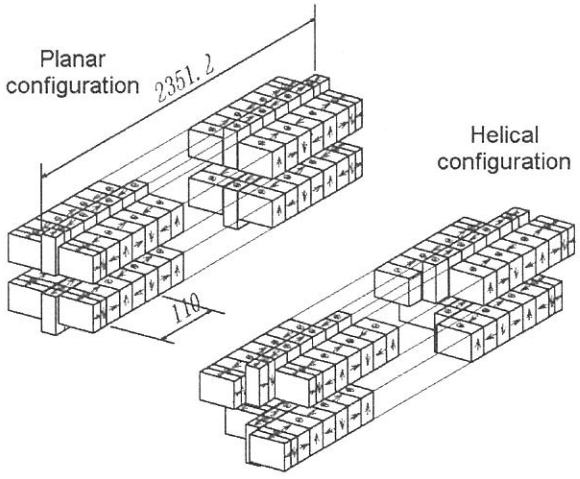

Fig. 1. Schematic figure of the UVSOR helical undulator in the planar and helical configurations.

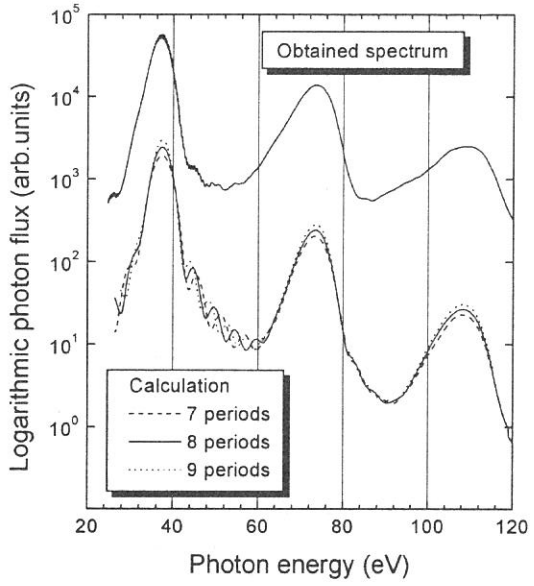

Fig. 2. Obtained (upper curve) and calculated (lower curves) spectra from the undulator at the undulator gap of 100 mm. The analytical calculation was done by using the parameters of the acceptance angle of 0.4 mrad and of 7, 8 and 9 periods of the magnet array. Note that the intensities of calculated spectra are shifted from the measured one for making the figure easier to read.

The observed spectrum at the undulator gap of 100 mm is shown in the upper part of Fig. 2. The fundamental radiation was observed at the photon energy of 37 eV, and the second and the third harmonics were also observed. In the case of the on-axis spectrum from the circularly polarized undulator radiation, the higher order components should not appear. In our experimental set-up for the performance test, however, not only the on-axis component but also the off-axis one of the undulator radiation was detected. Therefore the higher harmonics were observed in the spectrum.

Note that the observed spectrum was obtained by using the rearranged magnet array of the helical optical klystron for a helical free electron laser. In the optical klystron configuration, three periods at the center of the magnet arrays are rearranged [6]. By using the optical klystron, the shortest free electron laser wavelength of 239 nm was achieved [7]. As shown in Fig. 2, the interferogram appears in the fundamental radiation because of the use of the magnet array of the optical klystron. The interferogram is due to the interference of radiation from the former nine periods with that from the latter nine periods.

The analytical calculation results of the undulator spectrum with three different numbers of periods (7, 8 and 9 periods) are plotted in the lower part of Fig. 2. The best-fit spectrum of the analytical calculation was obtained with eight periods of undulator despite the nine periods of the undulator, and the acceptance angle of 0.4 mrad. The result means that the undulator radiation consists of the emissions from each center eight periods of the former and the latter magnet arrays. According to the calculation of the electron beam trajectory, the trajectories at the first and the last periods are far from the on-axis. Therefore the emission from the half of the first and the half of the last periods is not considered to interfere with the emission from the other periods. The value of 0.4 mrad is consistent with the maximum of the angular distribution of the undulator with eight periods.

References

[1] M. Kamada *et al.*, Rev. Sci. Instrum. **66**, 1537 (1995).
[2] N. Takahashi *et al.*, Jpn. J. Appl. Phys. **35**, 6314 (1996).
[3] X. M. Maréchal *et al.*, Rev. Sci. Instrum. **66**, 1937 (1995).
[4] T. Tanaka and H. Kitamura, J. Electron Spectrosc. Rel. Phenom. **80**, 441 (1996).
[5] S. Kimura *et al.*, J. Electron Spectrosc. Rel. Phenom. **80**, 437 (1996).
[6] H. Hama, Nucl. Instr. and Meth. in Phys. Res. A **375**, 57 (1996).
[7] K. Kimura *et al.*, UVSOR Activity Report 1996, 42 (1997).

(BL5B)

Reflectance of Mo/Si and Mo/C Multilayered Mirrors for the Double Multi-Layered-Mirror Monochromator of Beamline BL-4A1

Harutaka Mekaru[A] and Tsuneo Urisu[B]

[A]The Graduate University for Advanced Studies,
[B]Institute for Molecular Science, Myodaiji, Okazaki 444-8585

Multilayer structures of molybdenum/silicon and molybdenum/carbon have been shown to have high reflectivities in the extreme ultraviolet and , therefore, potential for use as monochromator elements. The authors developed a double multilayered mirror (MLM) monochromator and set up it as the part of the beamline BL-4A1 at the UVSOR for studies of synchrotron radiation (SR) stimulated processes.
We had measured the reflectivity of a multilayered mirror using monochromatized SR from the beamline 5B and reported here that we could estimated MLMs for use monochromator elements.

Figure 1(a) shows the experimental and calculated reflectivities of the Mo/Si MLM. A experimental reflectivity of 25.5% at the photon energy of 73eV and a normal incident angle of 40 degree demonstrated in the experimental data (solid curve) and the calculated one (dashed line). Figure 1(b) shows the experimental and calculated reflectivities of the Mo/C MLM. A reflectivities of 11.2% at the photon energy of 101eV and a normal incident angle of 30 degree and the calculated one.

The calculated reflectivity of the Mo/Si MLM showed the same peak energy of around 73eV as experimental one and that of the Mo/C MLM showed almost the same peak energy of around 97eV of the Mo/C MLM. However, the experimental reflectivity of a Mo/Si MLM is about 50.5% of the calculated value (50.5%) and that of a Mo/C MLM is about 85.3% of the calculated one (13.1%). These are because we did not think effects of the interface roughness and diffuseness layers on calculation.

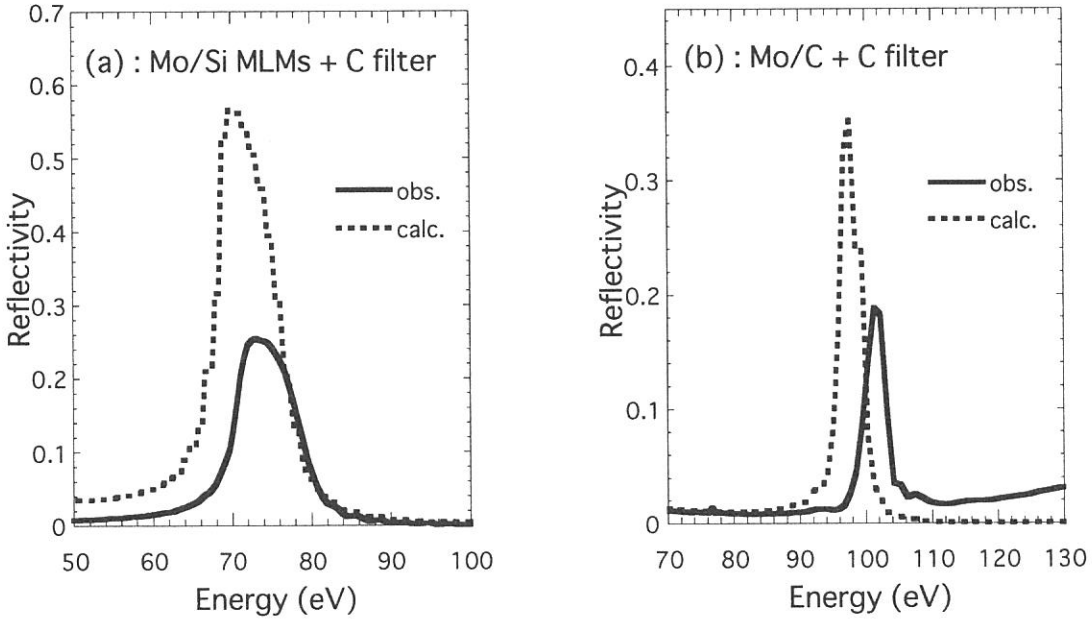

Figure 1 Experimental and calculated reflectivities of the Mo/Si MLM (a) and the Mo/C MLM (b).

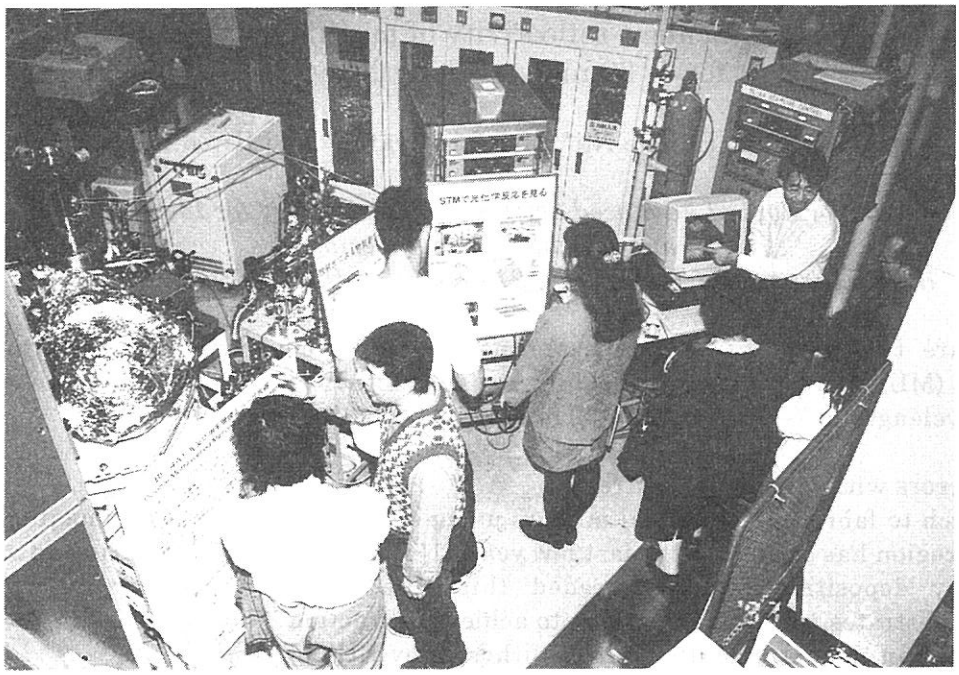

"What's going on BL4A and 4B"

"Open House" on Nov. 15

"Coincidence, that is the question"

"Open House" on Nov. 15

(BL5B)

Normal incident reflectivity of multilayer mirrors for 7- 20 nm wavelength region

Masahito Niibe, Hajime Nii* Atsushi Miyafuji* and Hiroo Kinoshita

Laboratory of Advanced Science and Technology for Industry
*and *Faculty of Engineering,*
Himeji Institute of Technology, 2167 Shosha, Himeji, Hyogo 671-2201

There are two purposes in this experiment. One is measuring reflectivity of Mo/Si multilayer (ML) mirrors with low residual stress. Another is measuring reflectivity of MLs for the wavelength of 7-10 nm and 16-20 nm regions.

I. ML mirrors with low residual stress

A research to fabricate aspherical mirrors using deposition methods for imaging optics in soft X-ray region has started in the last few years[1]. The technology is figuring an aspherical surfaces by depositing laterally graded thin film on a spherical substrates, and it is important to achieve diffraction limit resolution in extreme-ultra-violet lithography(EUVL) optical system. We used ML films instead of single layer films for the deposition films because surface of the ML is very smooth to avoid scattering of X-rays by surface roughness. However the ML typically have a residual stress of 200 MPa (compressive) that is high enough to deform the figure of precision substrates for the imaging optics.

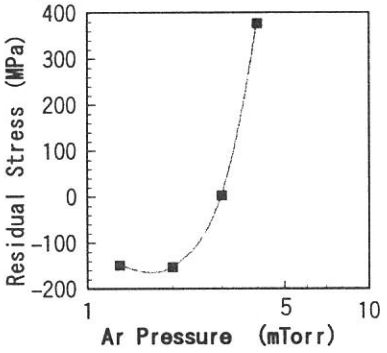

Fig. 1 Stress in Mo/Si MLs

We have been able to reduce the residual stress of the ML films to almost zero by optimizing a deposition condition of rf-enhanced-plasma magnetron sputtering system. Figure 1 shows Ar gas pressure(PAr) dependence of residual stresses in Mo/Si MLs. The residual stress was reduced to zero at PAr=3 mTorr.

We measured normal incidence reflectivity of the MLs prepared under various Ar pressure. The measurement was carried out at BL5B (radiometric calibration beam line) in UVSOR.

The reflectivity spectrum of ML at PAr=3 mTorr is shown in Fig. 2(diamond). The peak reflectivity was over 50% and the value was almost equal to that of the ML with high quality surface deposited at PAr=1.3 mTorr (dotted)[2]. So we concluded that ML in zero stress is not inferior to the ML for high reflectivity.

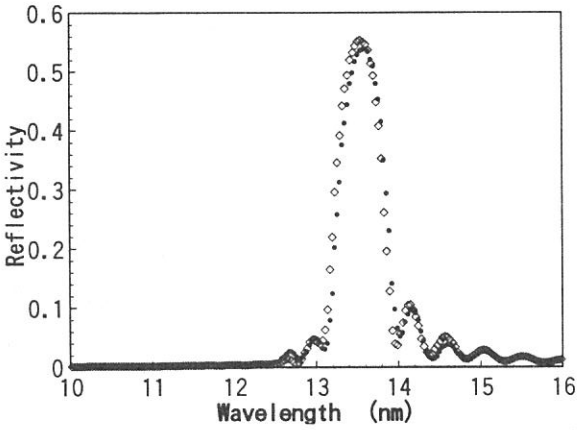

Fig. 2 Reflectivity of Mo/Si MLs deposited at PAr=1.3 mTorr (dotted) and 3 mTorr (diamond).

II. Reflectivities of MLs for the wavelength of 7- 10 nm and 16-20 nm regions.

Mirrors with high reflectivity at normal incidence for the soft X-ray and extreme-ultra-violet(EUV) wavelength regions would be useful for a number of applications, including synchrotron radiation optics. To date, Mo/Si ML mirrors have given the best results in the wavelength region that extends from 12 to 16 nm, and peak reflectivity of 65% at λ =13 nm have been achieved. However, below and above these wavelengths no material pairs have been found that yield comparable results.

Recently, mirrors for the 7-10 nm and 16-20 nm wavelength regions became very important

because of the application in X-ray microscopy and X-ray lasers. A theoretical search has shown that B4C-based MLs, such as Pd/B4C, Rh/B4C and Ru/B4C, and Al-based MLs, such as Mo/Al, could ideally give normal-incidence peak reflectivities ranging from 35% to 52% at λ =7-10 nm and 60% at λ =18.5 nm regions, respectively.

Rh/B4C and Mo/Al ML mirrors were fabricated by rf magnetron sputtering system under different deposition conditions. They were characterized by reflectivity measurements at normal and grazing angle of incidence. Figure 3 shows the reflectivity spectrum of the Rh/B4C ML mirrors measured at 7 - 10 nm wavelength region. Normal-incidence peak reflectivities of 10.5%, 11.2% and 20.2% were obtained at wavelengths of 7.7, 9.2 and 10.3 nm, respectively. Figure 4 shows the reflectivity spectrum of the Mo/Al ML mirror. Normal-incidence peak reflectivities was measured to be 17% at wavelength of 18.5 nm.

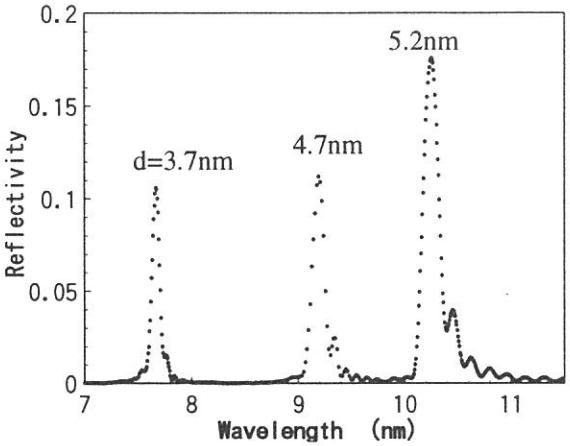

Fig. 3 Reflectivity of Rh/B4C ML mirrors at an angle of incidence of 5 deg.

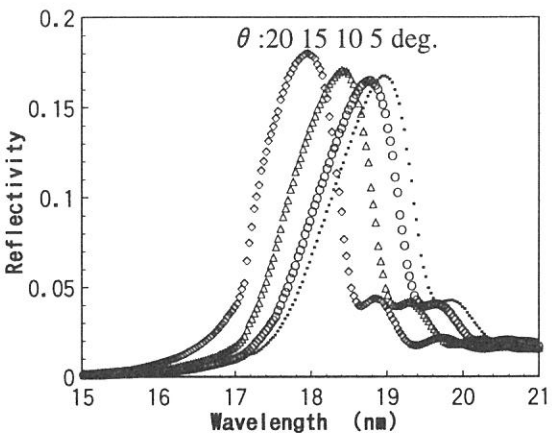

Fig. 4 Reflectivity of a Mo/Al ML mirror at angles of incidence of 5, 10, 15 and 20 deg.

III. Evaluation of higher order lights at BL5B monochromator

X-rays from a grating monochromator contains higher order lights of a grating. Even if suitable filters are used, higher order lights cannot completely be suppressed. In order to evaluate the contributions of higher orders, we measured reflectivity of a ML as function of wavelength.

Figure 5 shows the observed reflectivity of a Rh/B4C ML for wide wavelength range with no filter. Used combination of grating and mirror of the PGM monochromator was G2-M2. Angle of incidence was fixed to 10 deg. The first order Bragg reflection occurs at λ =7.5 nm. Observed reflectivity peaks at longer wavelength are due to the first order Bragg reflection of higher order lights from the grating.

From the result, the ratio of higher order contribution to the first order was estimated to be 0.2 at λ =15 nm.

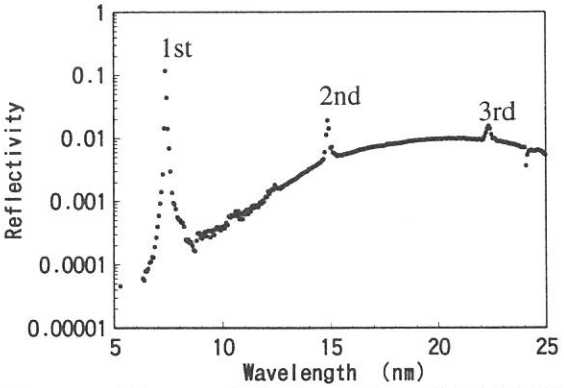

Fig. 5 Observed Reflectivity of Rh/B4C ML for 5-25 nm wavelength region.

[1] M. Niibe et al. : Jpn. J. Appl. Phys., 36 (1997) pp. 7601-7604.
[2] M. Niibe et al. : Rev. Laser Eng., 24 (1996) pp.48-60.

(BL5B)

Development of Novel Soft X-Ray Optics with Oxide Multilayer Structures

Hiroshi Kumagai, Katsumi Midorikawa, Sohachi Iwai[A] and Katsunobu Aoyagi[A]

Laser Technology Laboratory,
The Institute of Physical and Chemical Research (RIKEN),
2-1 Hirosawa, Wako, Saitama 351-0198, Japan
[A] *Semiconductor Laboratory,*
The Institute of Physical and Chemical Research (RIKEN),
2-1 Hirosawa, Wako, Saitama 351-0198, Japan

Development of high-performance normal-incidence multilayer optics for the *water-window* wavelength region between the oxygen and carbon K absorption edges at 2.33 and 4.36 nm, respectively, where water is relatively transmissive and organic materials are absorptive, has been a technical challenge of great interest. The extremely small periods (1.2-2.2 nm) of soft-X-ray reflectors require very rigorous specifications to be met with respect to interface roughness and interlayer mixing, because interface roughness on an atomic scale has a substantial effect on soft-X-ray reflectance. Therefore, the highest reflectance achieved at *water-window* wavelengths has been 3.3%,[1] in spite of the various efforts which have been made in this field. The reason that the reflectances achieved at these wavelengths are so low is that the Fresnel coefficients of materials are so small at these wavelengths that a large number of bilayers must be used, which means that the problems of interface roughness and imperfect interfaces due to interlayer mixing become serious.

The authors have proposed the use of a novel metal oxide multilayer, whose material combination is the same as that used in free electron lasers, for soft-X-ray reflectors at *water-window* wavelengths,[2,3] because an oxide multilayer can prevent the forming of an alloy at the interface, and the absorption of oxygen in oxides is negligible at the *water-window* wavelengths; moreover, the metal oxide multilayer can be fabricated by the atomic layer deposition or atomic layer epitaxy technique. These techniques can be used to control surfaces on an atomic scale by sequentially dosing the surface with appropriate chemical precursors and then promoting surface chemical reactions which are inherently self-limiting. We have found that the self-limiting adsorption mechanism works in the fabrication of oxide thin films such as aluminum oxide and titanium oxide.[4-6]

We report here on reflectance performances of novel metal oxide multilayers of titanium oxide and aluminum oxide using monochromatized synchrotron radiation (SR) from the beamline 5B of the 750-MeV electron storage ring located at the Ultraviolet Synchrotron Radiation Facility (UVSOR).

Figure 1 shows the experimental and calculated results of incidence-angle dependence on reflectances of the aluminum oxide/titanium oxide multilayer fabricated by the atomic layer deposition method of controlled growth with sequential surface chemical reactions. A high reflectance (s-polarization) of 33.4% at the wavelength of 2.734 nm and an incident angle of 71.8° from the normal incidence are

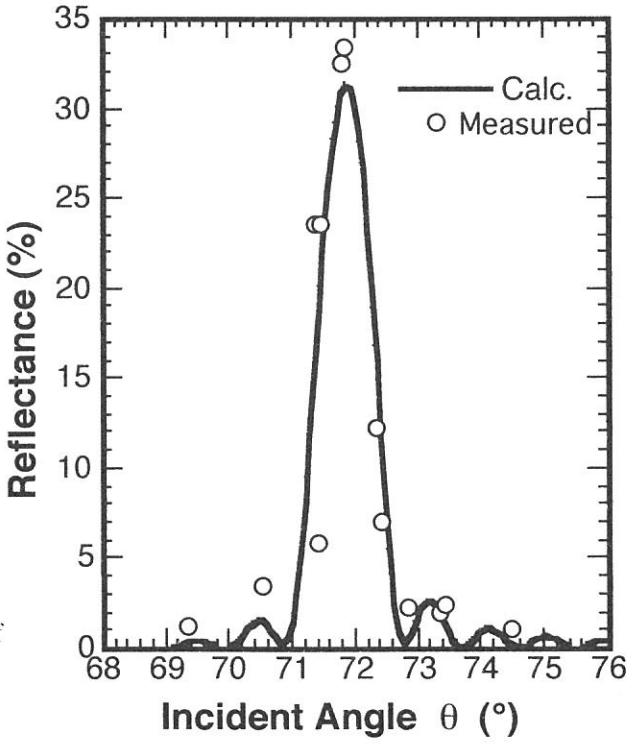

Figure 1 Experimental and calculated results of incidence-angle dependence on reflectances of the aluminum oxide/titanium oxide multilayer.

demonstrated in the experimental plots, which were obtained using the monochromatized SR. The calculated reflectance (solid line) shows almost the same reflectance of around 32% as the experimental one. Full width of the half maximum of the reflectance at 71.8° is about 1.0°.

Figure 2 shows the experimental and calculated profiles of reflectances of the aluminum oxide/titanium oxide multilayer fabricated by the atomic layer deposition method of controlled growth with sequential surface chemical reactions. Although the bilayer thickness is as short as 2.6nm and the period is 40, high reflectance (s-polarization) of 15.8% at the wavelength of 2.734 nm and an incident angle of 58.5° from the normal incidence are demonstrated in the experimental plots. The calculated reflectance (dashed line) shows a reflectance of 20.3%. The descrepency between experimental and calculated reflectances arises from the surface and interface roughnesses.

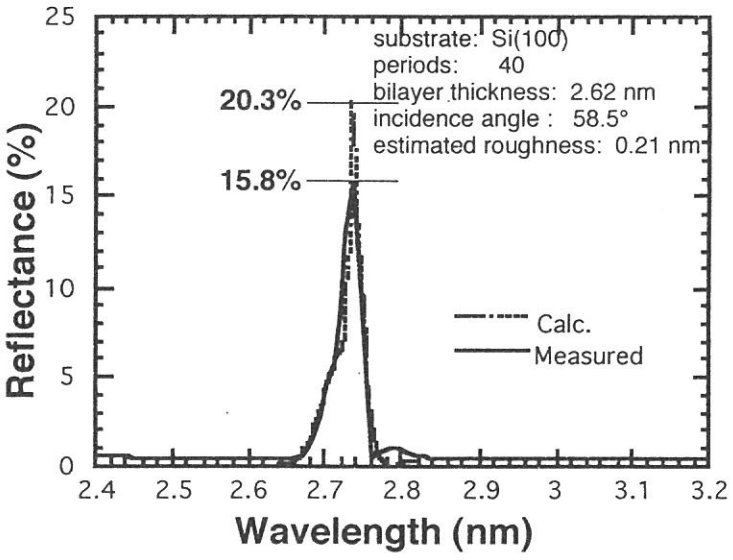

Figure 2 Eexperimental and calculated profiles of reflectances of the aluminum oxide/titanium oxide multilayer.

This work was supported by the Joint Studies Program (1997) of the Institute for Molecular Science.

References

1) I. V. Kozhevnikov, A. I. Fedorenko, V. V. Kondratenko, Yu. P. Pershin, S. A. Yulin, E. N. Zubarev, H. A. Padmore, K. C. Cheung, G. E. van Dorssen, M. Roper, L. L. Balakireva, R. V. Serov and A. V. Vinogradov, Nuclear Instruments and Methods in Physics Research **A 345**, 594 (1994).
2) H. Kumagai, K. Toyoda, K. Kobayashi, M. Obara and Y. Iimura, Appl. Phys. Lett. **70**, 2338 (1997).
3) H. Kumagai, M. Matsumoto, Y. Kawamura, K. Toyoda and M. Obara, Jpn. J. Appl. Phys. **33**, 7086 (1994).
4) H. Kumagai, K. Toyoda, M. Matsumoto and M. Obara, Jpn. J. Appl. Phys. **32**, 6137 (1993).
5) H. Kumagai and K. Toyoda, Appl. Surf. Sci. **82/83**, 481 (1994).
6) H. Kumagai, M. Matsumoto, K. Toyoda, M. Obara and M. Suzuki, Thin Solid Films **263**, 47 (1995).

(BL5B) **X-ray phase compensation in multi-periodic structure; strict reflection-wavelength control method for short periodic multilayer mirrors**

Masashi Ishii, Sohachi Iwai, Tatzuo Ueki and Yoshinobu Aoyagi
The Institute of Physical and Chemical Research (RIKEN), Wako-shi Saitama 351-0198

The shortening of the reflection wavelength of multilayer mirrors, is an important requirement for future X-ray applications.[1-4] Recently, atomic layer epitaxy (ALE) has been adopted to produce X-ray multilayer mirrors[5]. In ALE, since the epitaxial growth is automatically stopped at 1 monolayer (ML) due to a 'self-limiting mechanism',[6-9] ALE has great potential for the realization of the short period multilayer optics with atomically abrupt interfaces. But despite this, the reflection wavelengths of multilayer mirrors fabricated by ALE becomes discrete, since the periodic length is discrete according to the layer-by-layer growth. In this report, we describe a new wavelength control method using a phase compensation in multi-periodic structure[10]. Reflection properties of multi-periodic structure produced by metalorganic vapor phase epitaxy (MOVPE) indicate that this method enables us to design the X-ray mirror with a selectable reflection wavelength by combination of layer-by-layer grown of films with various periodic lengths.

The concept of the multi-periodic structure to control the reflection wavelength shown in Fig. 1 is an example of the multi-periodic mirror with the reflection wavelength halfway between reflection wavelength of $(AlP)_2(GaP)_2$, $\lambda_{2,2}$, and that of $(AlP)_3(GaP)_2$, $\lambda_{3,2}$. Fig. 1 (a) and (c) indicate normal periodic structures of $(AlP)_2(GaP)_2$ and $(AlP)_3(GaP)_2$, with periodic length of $d_{2,2}$ and $d_{3,2}$, respectively. In the case of (a), the X-ray phase is same after passing through $d_{2,2}$ as shown by the closed circles, so that X-rays reflected at interfaces constructively interfere, resulting in an overall reflection at the wavelength, $\lambda_{2,2}$. Similarly, the X-ray with $\lambda_{3,2}$ is reflected in the case (c). In contrast with these structures, Fig. 1 (b) shows the multi-periodic mirror, in which the 1 period is composed of two parts, $d_{2,2}$ and $d_{3,2}$. Although the X-ray with the wavelength of $(\lambda_{2,2} + \lambda_{3,2})/2$, has a phase lag after passing through the period $d_{2,2}$ as shown by the open circle, it reverts to the same phase as initial one at the end of the next $d_{3,2}$ period. Thus the $d_{3,2}$ compensates the phase lag of $d_{2,2}$. This phase compensation results in X-ray diffraction, and an X-ray mirror at $(\lambda_{2,2} + \lambda_{3,2})/2$ may be realized. For the sake of convenience, this multi-periodic structure, $[(AlP)_2(GaP)_2]_1[(AlP)_3(GaP)_2]_1$ is represented by $(2,2)_1(3,2)_1$ in the following discussion. Fig. 2 indicates the calculated reflectivity of $(2,2)_1(3,2)_1$, along with those of $(AlP)_2(GaP)_2$ and $(AlP)_3(GaP)_2$. A sharp reflection peak midway of $\lambda_{2,2}$ and $\lambda_{3,2}$, is clearly seen with no other reflection signal obtained in this wavelength range. Fig. 3 is an amplitude reflectance of $(2,2)_1(3,2)_1$ calculated at $(\lambda_{2,2} + \lambda_{3,2})/2$. As shown in this figure, zigzag interface phase caused by the two periodic lengths is observed. This zigzag phase indicates that the X-ray phase is compensated at the interface, agreeing with the qualitative explanation in Fig. 1 (b). Since this concept does not depend on optical constants, if multilayer mirrors with other more optically favorable materials can be fabricated by ALE, a similar discussion will be applied to new materials.

In order to discuss actual phase compensation properties, the multi-periodic structure is fabricated by using MOVPE system which has a cold-wall-type horizontal quartz reactor with a RF heating system. Tertiarybutylphosphine (TBP) was used as the group-V source gas. Triethylgallium (TEG) and dimethylaluminum hydride (DMAH) were alternatively introduced into the growth chamber for the growth of GaP and AlP, respectively. The periodic length is controlled by variation of the TEG feeding time. The substrates were (100)-oriented nondoped GaP which were chemically treated in $(NH_4)_2S_x$ solution. The X-ray reflectance was measured using monochromatized synchrotron radiation (SR) from the 750 MeV electron storage ring located at the Ultraviolet Synchrotron Radiation Facility (UVSOR).

Fig. 4 (b) indicates the reflection propertiy of the multi-periodic structure in which the 1 period is composed of two AlP/GaP layers with different thickness of 2.3 and 3.0 nm. Note that the difference of these periodic lengths is only a few monolayers. The reflectance of normal AlP/GaP multilayer structures with single periodic lengths of (a) 2.3 nm, (c) 3.0 nm and (d) 5.3 m, is also shown in this figure. These reflectance are normalized by that of the

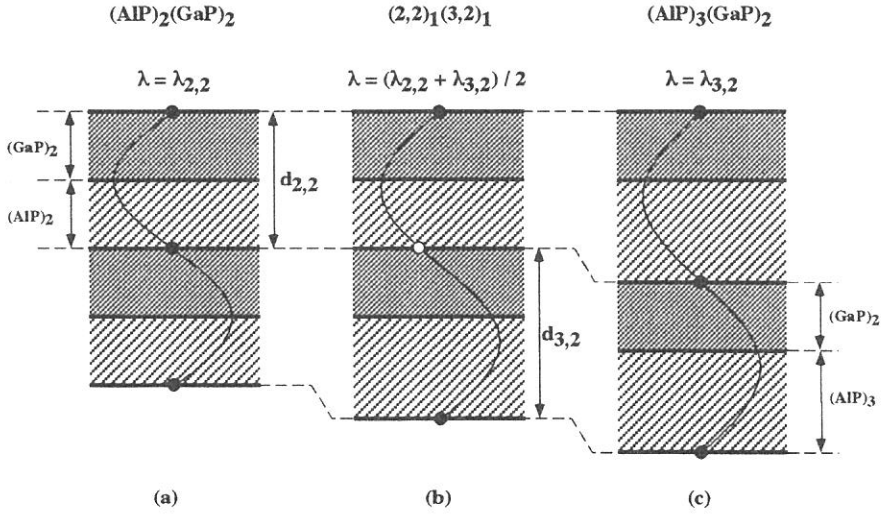

Fig. 1 The concept of the multi-periodic structure to control the reflection wavelength

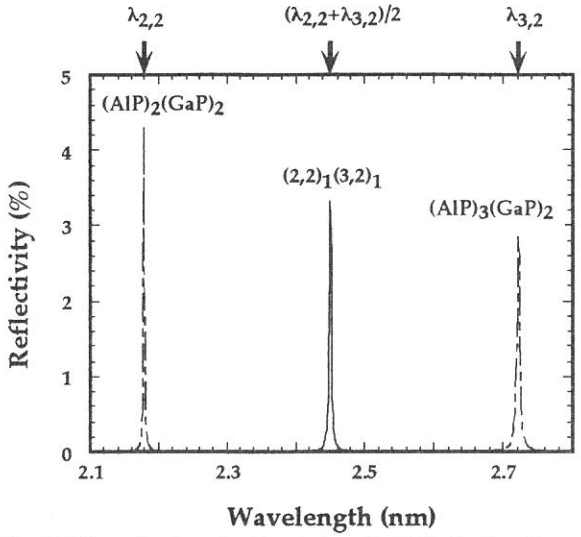

Fig. 2 The calculated reflectivity of $(2,2)_1(3,2)_1$, along with those of $(AlP)_2(GaP)_2$ and $(AlP)_3(GaP)_2$

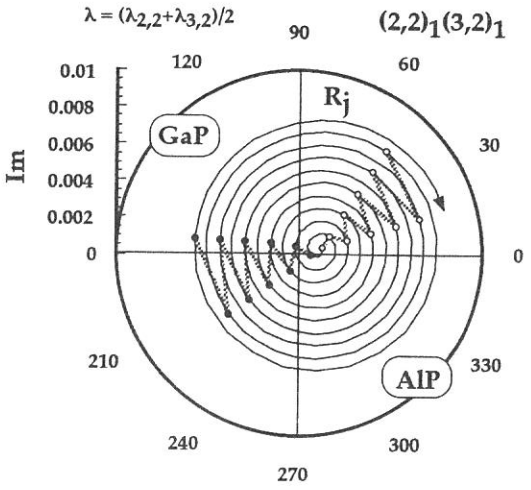

Fig. 3 The amplitude reflectance of $(2,2)_1(3,2)_1$ calculated at $(\lambda_{2,2} + \lambda_{3,2})/2$

multi-periodic structure. The incidence angle is fixed at 27° . A reflection peak midway of (a) and (c) caused by the phase compensation is clearly observed. Moreover, the reflection loss by this compensation is quite low, so that it acts just as a normal multilayer mirror with the middle periodic length of (2.3 + 3.0)/2. On the other hand, the reflectance of (d) caused by $2d \sin\theta = 2\lambda$ is low, indicating that the reflection of the multi-periodic structure is essentially different from the higher order diffraction. The comparison of X-ray phase between the multi-periodic reflection and higher order diffraction was discussed in another paper[10]. The reflection wavelength of the multi-periodic mirror is determined by the combined ratio of the periodic layers. Based on this simple combination rule, a strict reflection wavelength control without the interface roughness is expected to be realized by multi-periodic structures fabricated by ALE.

In summary, an X-ray phase compensation as a new reflection wavelength control method for layer-by-layer controlled multilayer mirrors is proposed. The phase compensation is clearly observed in reflection properties of multi-periodic structure produced by MOVPE. The multi-periodic structures fabricated by ALE are expected to act as short-wavelength x-ray mirrors without interface roughness.

[1] D. G. Stearns, R. S. Rosen and S. P. Vernon: Opt. Lett. 16, 1283 (1991).
[2] J. F. Seely, G. Gutman, J. Wood, G. S. Herman, M. P. Kowalski, J. C. Rife and W. R. Hunter: Appl. Opt. 32, 3541 (1993).
[3] C. Montcalm, B. T. Sullivan, M. Ranger, J. M. Slaughter, A. Kearney, C. M. Falco and M. Chaker: Opt. Lett. 19, 1004 (1994).
[4] I. V. Kozhevnikov, A. I. Fedorenko, V. V. Kondratenko, Y. P. Pershin, S. A. Yulin, E. N. Zubarev, H. A. Padmore, K. C. Cheung, G. E. van Dorssen, M. Roper, L. L. Balakireva, R. V. Serov and A. V. Vinogradov: Nucl. Instr. and Meth. in Phys. Res. A345, 594 (1994).
[5] M. Ishii, S. Iwai, T. Ueki and Y. Aoyagi: J. Cryst. Growth 180, 15 (1997).
[6] J. Nishizawa: J. Electrochem. Soc. 132, 1197 (1985).
[7] Y. Aoyagi: J. Vac. Sci. Technol. B5, 1460 (1987).
[8] M. Ishii, S. Iwai, T. Ueki and Y. Aoyagi: Appl. Phys. Lett. 71, 1044 (1997).
[9] M. Ishii, S. Iwai, T. Ueki and Y. Aoyagi: Thin Solid Films (in press).
[10] M. Ishii, S. Iwai, T. Ueki and Y. Aoyagi: Appl. Opt. 36, 2152 (1997).

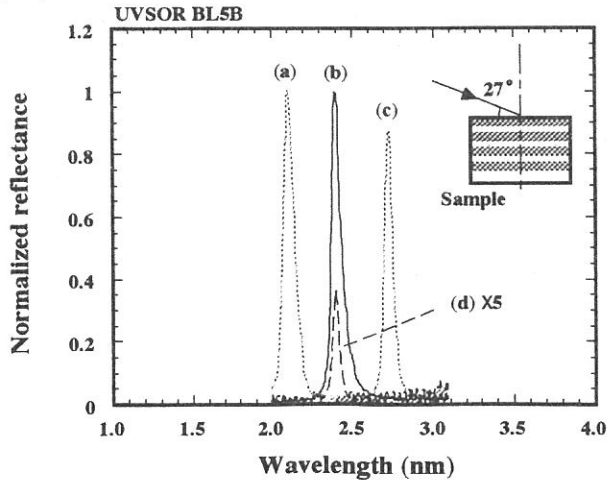

Fig. 4 Reflectance of various samples produced by MOVPE. The periodic lengths are (a) 2.3, (c) 3.0 and (d) 5.3 nm. (b) is the multi-periodic structure in which the 1 period is composed of two AlP/GaP layers with different thickness of 2.3 and 3.0 nm.

(BL5B)

High Quality XUV Multilayer Mirror for XUV Doppler Telescope Aboard Sounding Rocket

Saku TSUNETA, Taro SAKAO, Hirohisa HARA, Toshifumi SHIMIZU,
Ryouhei KANO, Tsuyoshi YOSHIDA[1], Shin'ichi NAGATA[1],
Ken KOBAYASHI[1]

National Astronomical Observatory, 2-21-1 Osawa, Mitaka, Tokyo, 181, Japan
[1] *Department of Astronomy, School of Science, The University of Tokyo, Bunkyo-ku, Tokyo, 113, Japan*

We have been developing the high-quality XUV multilayer mirrors for the XUV telescope aboard the ISAS sounding rocket experiment over 3 years. The telescope consists of a Cassegrain multilayer optics with an X-ray CCD camera. The mission is (1) to obtain single temperature (1.8 MK) X-ray images of the Sun by isolating the specific emission line [Fe XIV line (211.3Å)], and (2) to obtain the Dopplergram of the solar corona with two normal incidence telescopes, whose peak wavelengths are slightly (about 2Å) shifted toward red and blue from the line. (The line moves in between the blue and red windows of the multilayer mirrors due to the motion of the plasma, and the velocity map of the 1.8MK plasma is obtained by subtracting the blue from the red images.)

In order to improve the detection limit of the velocity fields, and to avoid the contamination from the nearby emission lines, we need to develop a high-wavelength resolution mirror ($\lambda/\Delta\lambda \sim 40 - 50$) tuned for the 211Åline. Such a high wavelength resolution is realized by increasing the number of the layer pairs contributing to the reflectance, *ie* by selecting less-absorbing materials for both the reflector and the spacer, and by decreasing the thickness of the reflector. We have successfully developed the MoSi/Si multilayer mirror with system (two mirrors) wavelength resolution as high as 47 (Figure 1).

The multilayer coated on the large-area mirror inherently has large non-uniformity in the wavelength of the reflectivity peak owing to the radius-dependent distance from the sputtering source. This must be corrected with an accuracy of a few times 0.1Åover 15 cm diameter. We have measured the non-uniformity of the large-area sample mirror with UVSOR, and made a more uniform mirror with the correcting mask designed on the basis of the measurement. This iteration was repeated several times. The final uniformity is exceptionally good, and is within 0.1Åover the distance (Figure 2).

We have also developed the anti-reflection layer (light-trap) to the MoSi/Si mirror for the intense (X100) HeII line at 304Å. Fig. 1 also shows the sharp peak at 211Å, and the anti-peak near 304Å. The quantum efficiency of the flight CCD camera is also measured with UVSOR. Figure 3 shows the excellent performance of the Site back-illuminated CCD.

References (published in FY1997):

Hara, H., Kano, R., Nagata, S., Sakao, T., Shimizu, T., Tsuneta, S., Yoshida, T., Kosugi, K., XUV Doppler Telescope with multilayer optics, Proc. SPIE, Grazing incidence and multilayer X-ray optics, 3113, 420–429, 1997.

Ishiyama, W., Murakami, K., Tsuneta,S., Sakao, T., Hara, H., Shimizu, T., Yoshida, T., Nagata, S., Kano, R., Fabrication of multilayer mirrors for the XUV Doppler telescope for solar corona observation, Proc, The 4th International Conference on The Physics of X-Ray Multilayer Structures, in press, 1998.

Nagata, S., Hara, H., Sakao, T., Shimizu, T., Tsuneta, S., Yoshida, T., Ishiyama, W., Murakami, K., Oshino, T., Development of the multilayer mirrors for XUV Doppler telescope, Proc. SPIE, Grazing incidence and multilayer X-ray optics, 3113, 193–201, 1997.

(BL5B)

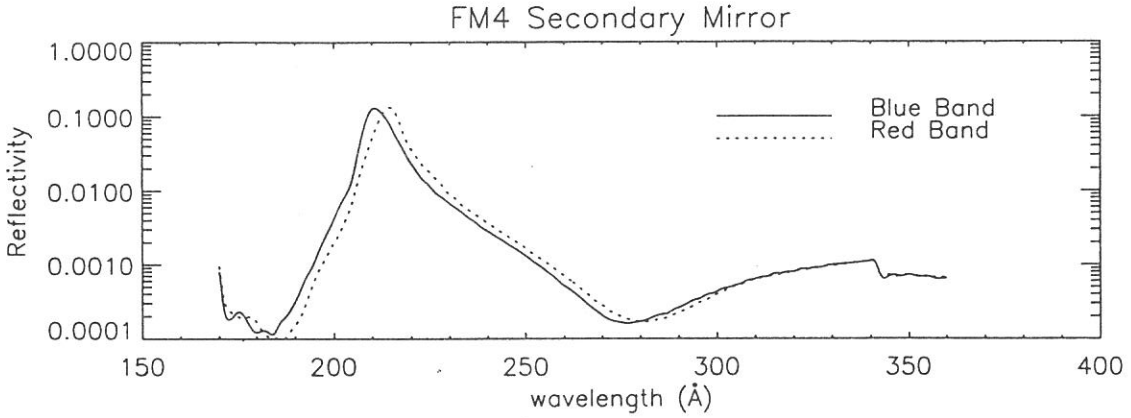

Figure 1: Measured reflectivity profile of the flight MoSi/Si (Γ =0.2) primary mirror. The secondary mirror has similar profile. The anti-peak around 304Åis due to the light-trap (single Si layer) to absorb the intense HeII line at 304Å, which is hazardous for the observation.

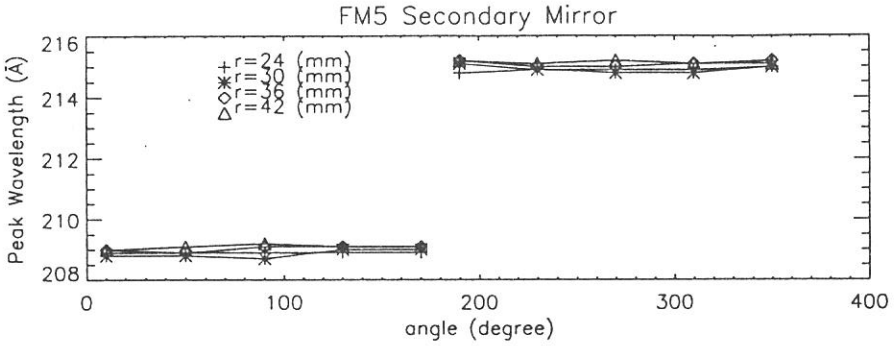

Figure 2: Exceptionally good uniformity of the flight mirror: peak wavelength as a function of the azimuth angle for various radius. The uniformity is within 0.1Å. The half of the mirror corresponds to the red passband, and the other half to the blue passband.

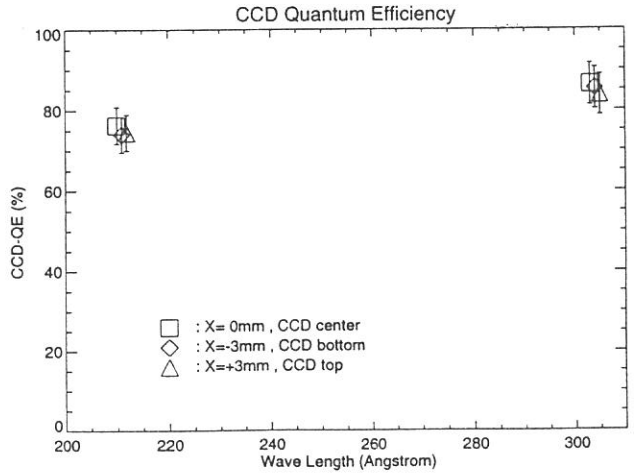

Figure 3: Quantum efficiency of the flight CCD camera measured with UVSOR. The CCD used here is the Site back-illuminated 512X512 CCD. The data shows the excellent performance of the CCD in XUV wavelengths.

(BL5B)

The Calibration of the eXtreme Ultra-Violet Scanner (XUV-S)

Masato Nakamura [A], Yoshiyuki Takizawa [A], Ichiro Yoshikawa [A],
Atsushi Yamazaki [A], Kei Shiomi [A] and Hiroko Hayashi [A]

[A] *Faculty of Earth and Planetary Science, University of Tokyo, Bunkyo-ku, Tokyo 113-0033*

Planet-B will be launched in July 1998 to the Mars and our designed eXtreme Ultra-Violet Scanner (XUV-S) is on board. The scanner will observe the resonantly scattered emissions of He atoms and He ions, HeI (584Å) and HeII (304Å) respectively, and analyze the distribution of He atoms and He ions in the plasmasphere of the Earth and the Martian atmosphere. The scanner consists of a thin metal filter, a multi-layer coated mirror and micro channel plates (MCPs) with CsI coating. The purpose of this our experiment at UVSOR is to measure the transmittance of the filter and the reflectivity of the mirror in the extreme ultra-violet region, especially at HeII (304Å).

From our last experiment result at UVSOR we know that the line of the grating and mirror setting for 304Å considerably contain the higher-order lines, for example the second order of 152Å. Therefore it is the first purpose that a pure 304Å line is guided into the chamber for calibration. For the reduction of the higher-order lines the guided line is transmitted a filter which has a very low transmittance only in the wavelength region of higher-order lines. Materials having the character are Aluminum and Magnesium. Al has very low transmittance below 170Å, and Mg below 250Å. So we use an Al/Mg filter for the purpose. The beam transmitted through an Al/Mg filter is guided into the chamber and grazed by using our grating on the center of the goniometer. Incident angle is 45 degree, and our detector is rotated and observes the grazed lines (Fig.1). The center spot of Fig.1 is the zero-order line, and both side spots are the plus and minus first order 304Å line. If there is a contamination of a higher-order line, a spot between the center and the side spots should be observed. But it is not showed on Fig.1, therefore the beam through an Al/Mg consist of only 304Å and is enough pure for our purpose. We consider this pure 304Å beam as the direct one and measure the transmittance of the filter and the reflectivity of the multi-layer coated mirror.

The filter for XUV divides two parts: the half consists of Al, the other half Al/C. Though the transmittance of Al for 304Å and 584Å are the same order, the transmittance of C for 304Å is much more than for 584Å. Therefore the part of the Al filter measures both HeI and HeII, and the part of the Al/C filter measures HeII. During the measurement of the transmittance, the detector MCPs for experiments is set on the place to detect directly the pure 304Å beam and the filter is set to interrupt the beam or not to. Alternately MCPs detect the transmitted beam and the pure direct beam, and the rate of the counts is the filter transmittance. The transmittance depended on wavelength (200 500Å) by using the GM35 of the goniometer is shown in Fig.2. The solid circle shows the transmittance of the Al/C filter, the open circle shows the Al filter and the solid and dash line shows the simulation value of the Al/C and Al filter respectively. Below 340Å the obtained shape of the transmittance is consistent with the simulation value, but over 340Å the difference between the measurement and the simulation value. It is thought that this is because the higher-order line is contaminated.

The mirror reflectivity is measured by using a photo diode because the MCPs have the dependence of the sensitivity on a incident angle of a beam. Also the reflected beam and the pure direct beam is detected by the photo diode, and the rate of the output current is the reflectivity. The dependence of the reflectivity on the wavelength (150 600Å) is measured by using the GM35, and shown in Fig.3. The

peak of the reflectivity is shown at the wavelength of 304Å, and it is shown that the coated multi-layer of the mirror is very well.

It is the future work to estimate the effect of the higher-order line and to measure the transmittance and the reflectivity at 584Å.

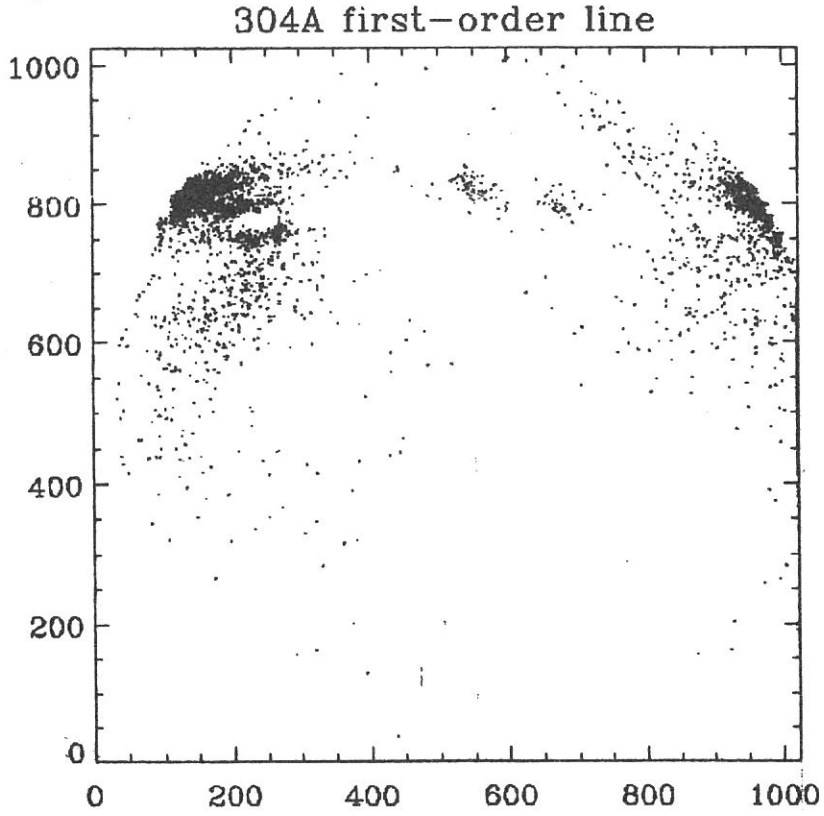

Fig.1 The line transmitting Al/Mg filter. The grazed line by using our grating consist only of 304Å, because no spot appears between the zero-order spot and the plus and minus first-order spot.

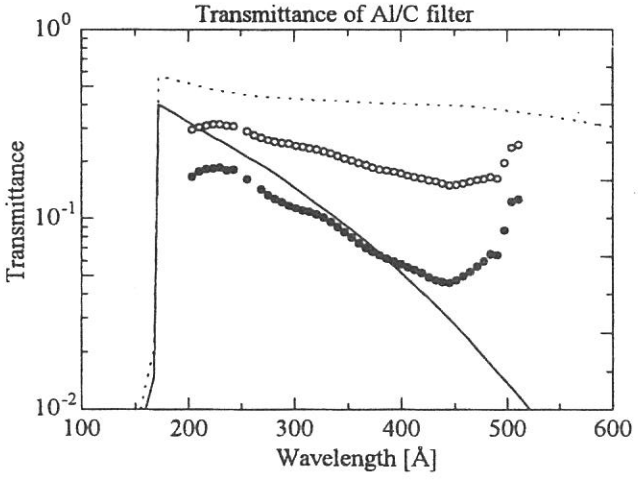

Fig.2 The transmittance of the filter Al and Al/C for XUV-S. The solid and open circle shows the transmittance of the Al and Al/C part of the filter, respectively.

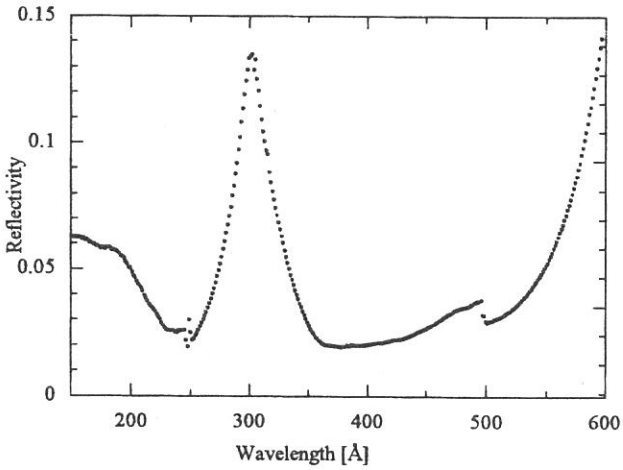

Fig.3 The reflectivity of the multi-layer coated mirror for XUV-S. The peak of the reflectivity is shown at the HeII emission (304Å).

(BL6A1)

Infrared magnetic circular dichroism experiment using synchrotron radiation

Shin-ichi KIMURA

UVSOR Facility, Institute for Molecular Science, Okazaki 444-8585

In vacuum-ultraviolet (VUV) and x-ray regions, synchrotron radiation (SR) is well known to be one of powerful light sources for the investigation of electronic and crystal structures of materials. The main reason is that there had been no continuous light source in their regions before. Recently, not only the high brightness of SR but also the good linear and circular polarizations is conventionally used because polarizations give us new informations.

In the infrared region, on the other hand, there are several continuous light sources using blackbody nature. The intensity is comparatively strong but the brightness is not so high. Since SR is much higher brightness than such ordinary light sources, infrared synchrotron radiation (IRSR) has been used for the investigation of optical properties of small size material and surface vibration. Recently, more than ten beam lines for IRSR are working or under construction. Almost all the beam lines are planned to do experiments of infrared microscopy and imaging [1]. IRSR has become a new field of SR science.

Another features of IRSR are polarization properties. Ordinary light sources have no polarization. Then linear polarizer and 1/4-lambda plate are needed to make linear and circular polarizations. Therefore the available energy range is limited by the optical elements. On the other hand, SR has polarization in itself. Therefore SR with linear or circular polarizations can cover wide energy range without optical elements. This is a useful property for the investigations of electronic structure near the Fermi level and

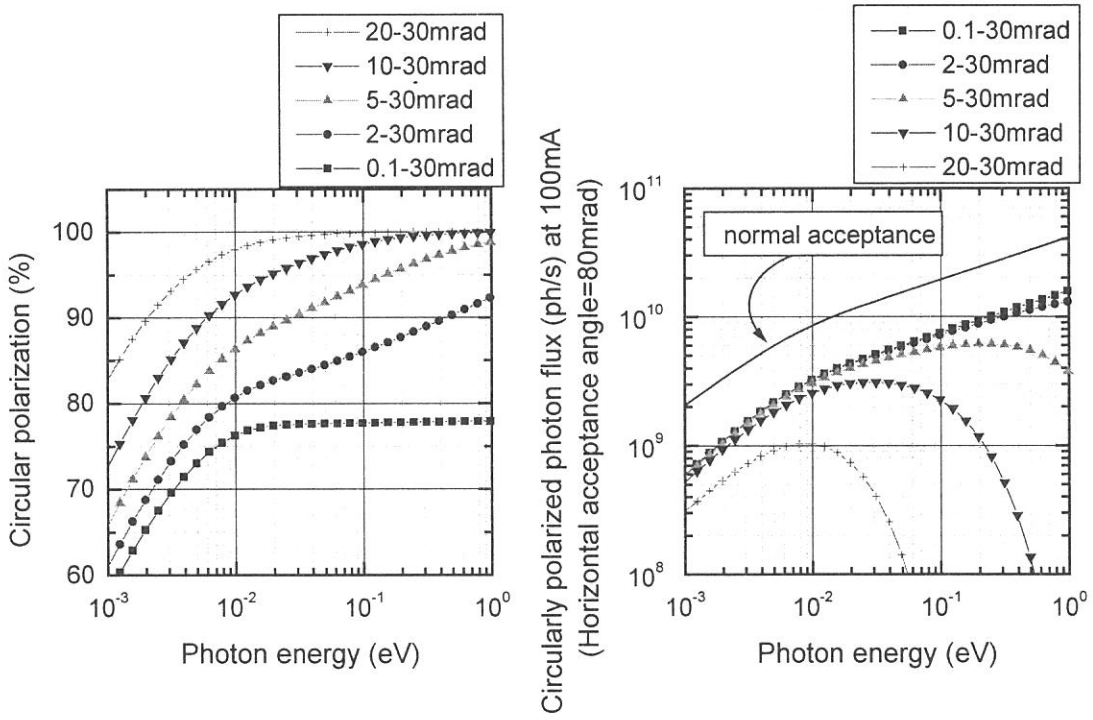

Fig.1. Expected circular polarization and circularly polarized photon flux of BL6A1 in several acceptance angles.

of the TO phonon band with circular dichroism.

According to the consideration, circular polarization and the effective intensity of IRSR from an infrared beam line, BL6A1, of UVSOR were calculated. The results are shown in Fig. 1. The vertical acceptance angle of BL6A1 is ±30 mrad. The acceptance angle is much larger than that of other VUV beam lines in UVSOR (typically ±4 mrad). The large acceptance angle gives us high circular polarization and high intensity in infrared region. The circularly polarized IRSR can be used in the energy range of 7 meV - 2 eV because it is limited by transmittance of beam splitters of a Michelson interferometer as mentioned below. Since the acceptance angle of 5 - 30 mrad is usually taken during circular polarization experiments, the polarization should be higher than 80 % and the intensity should be less than half of the case of normal experiment. Therefore we can use sufficient circular polarization and sufficient intensity in the photon energy range of 7 meV - 2 eV, which is available energy range at BL6A1.

Using the circularly polarized IRSR, the measurement of infrared magnetic circular dichroism (IRMCD) has been started. The main purpose is to investigate the coupling between carriers and magnetic moments of strongly correlated electron systems. The experimental setup is shown in Fig. 2. The optical system using the superconducting magnet is the infrared magneto-optical apparatus, which was constructed in the last fiscal year [2]. A Michelson-type FTIR interferometer (Bruker IFS66v) is used when the IRMCD experiment is done. There is a knife-edge depicted in Fig. 2 on the light pass to the interferometer. The upper or lower part of IRSR from UVSOR is picked up by the knife-edge and is derived to the interferometer. The light is guided to a sample mounted at the center of a superconducting magnet and to a detector by plane and parabolic mirrors. There are a lot of mirrors and one beam splitter. However the circular polarization of light was confirmed to be over 70 % at the detector position.

We measured IRMCD spectra of absorption of magnetic exciton of GdAs for instance. The results are presented in this issue [3].

References

[1] (e.g.) S. L. Hulbert and G. P. Williams, Sync. Rad. News **10**-1 (1997) 16.

[2] S. Kimura, UVSOR Activity Report 1996 (1997) p. 170.

[3] S. Kimura, D. X. Li, Y. Haga and T. Suzuki, in this issue.

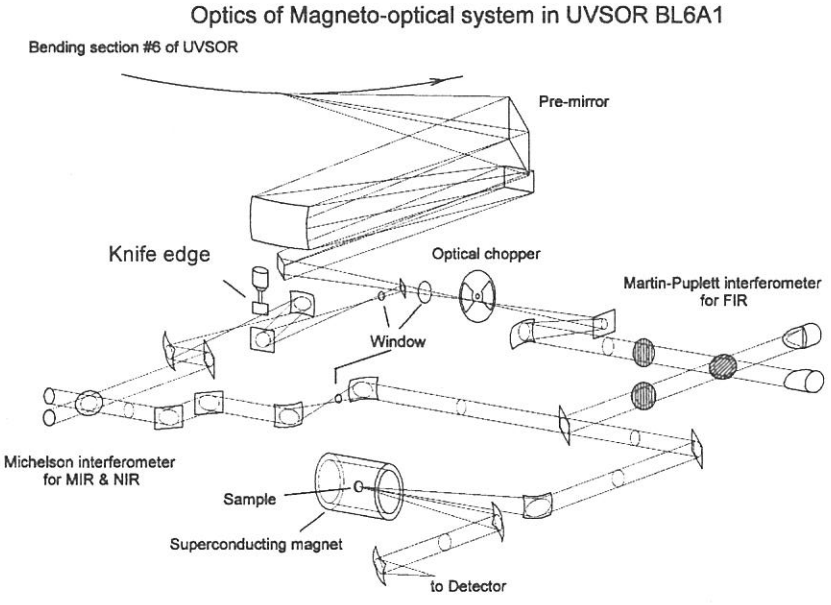

Fig. 2. Optical system of infrared magnetic circular dichroism measurement using SR at BL6A1.

(BL7A)

Focusing mirror system of the double crystal monochromator beamline BL7A

Toyohiko KINOSHITA, Tokuo MATSUKAWA[1] and Hiroaki YOSHIDA[2]

Institute for Molecular Science, Myodaiji, Okazaki 444-8585, Japan

[1]Department of Physics, Naruto University of Education, Naruto 772-8502, Japan

[2]Department of Material Science, Faculty of Science, Hiroshima University, Kagamiyama 1-3-1, Higashi-Hiroshima 739-8526, Japan

Since the first commissioning of the double crystal monochromator (DXM) beamline BL7A[1], the soft x-ray light from this beamline has been widely used by many users and been very invaluable for solid state spectroscopy. However, in recent few years, there exist some requirements concerning to the improvements of the beamline from the users. In order to satisfy the user's requirements and to get higher performance of the beamline, several improvements are now in progress, for example, renewing the computer control system, reconstruction of the big flange of the DXM chamber for easier exchange of the monochromator crystals, the use of YB_{66} monochromator crystal[2], installation of a wire beam monitor for easier alignment of the beamline and so on. The installation of the focusing mirror system is one of the big project among the improvements.

To provide higher photon flux in higher than 1keV photon energy region at BL7A, the superconducting magnet wiggler is installed in the straight section of the upper stream of the bending magnet section B7[3]. The wiggler is a wavelength shifter type and covers relatively higher photon energy range than normal bending magnet radiation. We use both the wiggler radiation and bending magnet radiation. When the higher energy light is used from the wiggler with crystals such as InSb(111) and Ge(111), the beam line is fixed just to the down stream of the straight section (0° line). In the case to use the SR from the bending section, the DXM accepts SR emitted at the point on the electron orbit downstream by 2° from the edge of the bending section. In order to avoid radiation damage to the insulator crystals such as beryl and quartz, we use the bending magnet radiation. The light of the photon energy rage from 1keV to 2keV is provided. Between the user's times of the wiggler radiation and the bending radiation, we have to exchange the beam line set up from 0° line to 2° line. Due to this exchange procedure, much beam time and much performance of the beamline have been lost.

In order to solve above problem, we designed the mirror system. The schematic drawing of the mirror system is shown in Fig. 1. Two pairs of the mirror system (total 4 mirrors) are installed in the chamber. The parameter value of each mirror is described in Table I. The "pair 1" and "pair 2" can be easily exchanged *in situ*. The system is installed in the downstream of the front end and the upper stream of the DXM chamber. The wiggler radiation is directly introduced to the straight line and reflected by one pair of the focusing mirrors to the vertical way. The output light comes out to the same direction as that of the incident light, but the height is 8mm higher. When we use the "pair 1", the higher energy light than 1.8keV will be reduced to less than 10% because of low reflectivity of Si in this condition. To cover the higher energy region, another "pair 2" coated by Cr will be used, which will show no structures in throughput spectrum at 700-5000eV region. The idea to reduce higher energy component of the light is similar to that reported in Ref. 4. The result of the ray tracing at the sample position for the "pair 2" system is shown in Fig. 2. The ray tracing was performed for the light of λ =15 Å. The result for the "pair 1" mirror is almost similar. As an option for the trouble of the wiggler itself, a port for the radiation from the bending magnet is also equipped.

By using this system, we may not need to move the beamline from the 0° line to 2° line . Higher photon flux and smaller spot size than the present ones can also be expected in conjunction with the wiggler radiation. It is expected that the reduction of the high energy component such as the glitches observed in the YB_{66} throughput[2] will become possible, when we use the pair of Si coated mirrors. These will give us a lot of advantages to perform soft x-ray spectroscopy measurements.

Acknowledgements

Authors would like to thank to the staff members of the UVSOR facility for the support.

References

1) T. Murata et al., *Rev. Sci. Instrum.* **63**(1992)1309.
2) T. Kinoshita et al., *J. Synchrotron Radiation*, in press: *UVSOR Activity Report* (1996) p. 198.
3) E. Nakamura et al., *J. Electron Spectrosc. Relat. Phenom.* **80** (1996) 421.
4) G. M. Lamble, *Rev. Sci. Instrum.* **66** (1995) 1422.

Table I. Parameters of the focusing mirror system. The substrate of the mirrors are quartz. M2 mirrors are located at 4900mm down stream from the center of the wiggler. These parameter values are for the focusing the beam to 8900mm down stream from the wiggler.

	coating	size	Incidence angle	Radius of the cylindrical mirror M1 for sagittal focusing	Radius of principle axes of the elliptic mirror M2 for meridional focusing
pair 1	Si	400(l)x35(w)x50(t) mm^3	89°	R=77.4(mm)	a=4450.07 (mm) b=77.27(mm)
pair 2	Cr	700(l)x35(w)x50(t) mm^3	89.5°	R=38.8(mm)	a=4450.03 (mm) b=38.63(mm)

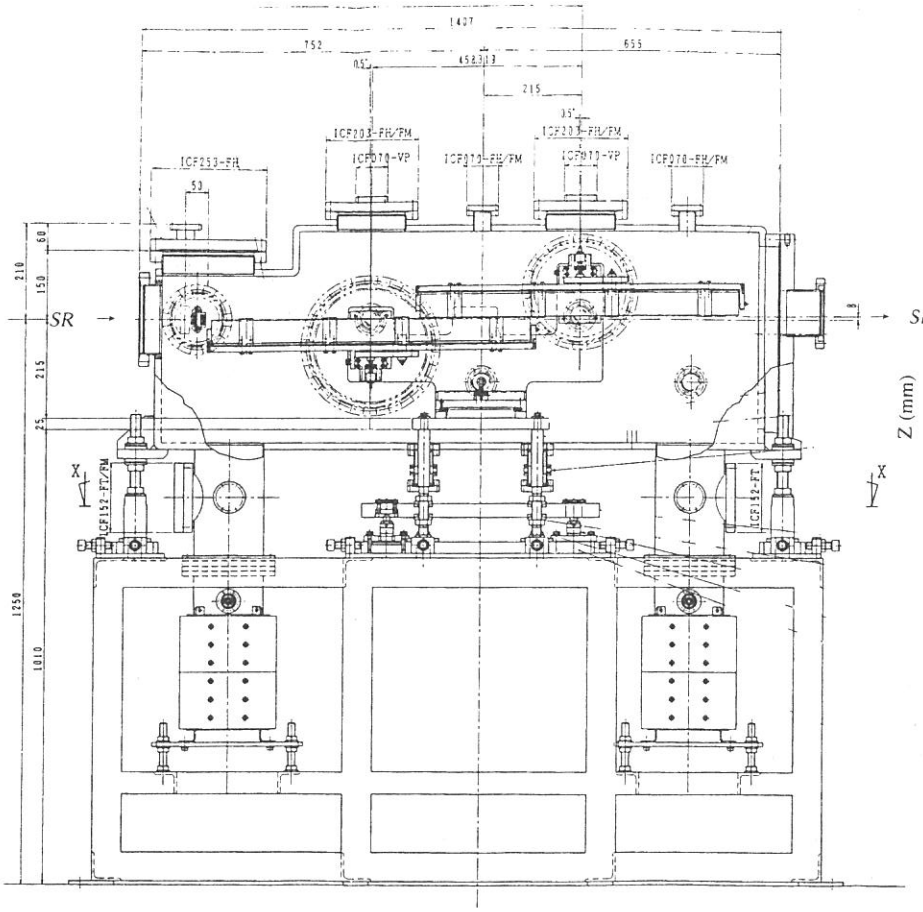

Figure 1. Schematic drawing of the focusing mirror system at BL7A.

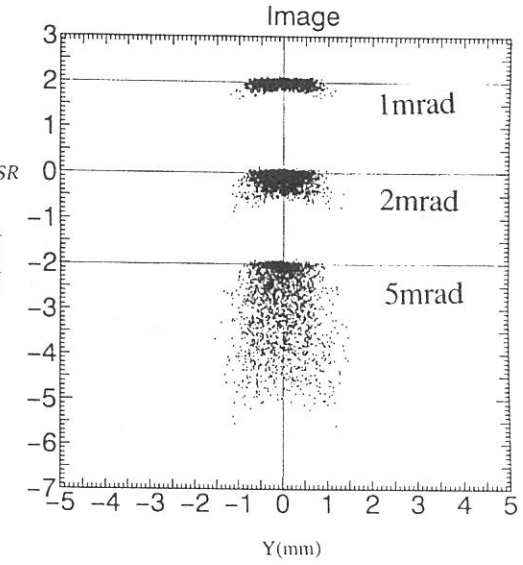

Figure 2. Result of the ray tracing at sample position for the "pair 2" mirror system. Depending on the horizontal acceptance angle of the wiggler radiation, the spot sizes are different.

(BL8B1)

Polarization diagnosis for BL8B1 and characterization of transmission multilayers for use around 65 eV

Tadashi Hatano, Weibing Hu, Masaki Yamamoto and Makoto Watanabe

Research Institute for Scientific Measurements, Tohoku University, Katahira 2-1-1, Aoba-ku, Sendai, 980-77, Japan

Since multilayers proved to be excellent polarizers when they are used at near pseudo-Brewster angle, soft x-ray multilayer polarizers have been rapidly developed. Multilayers work as phase retarders as well when the angle of incidence is readjusted appropriately. Multilayers of transmission type can be put into the optical path and rotated without varying the optical axis, which is remarkably helpful for the optics alignment. We designed and fabricated reflection and transmission multilayer polarizers of Al/YB_6 and Mo/Si for use in the 55~90 eV region to make measurements for magneto-optical effects around $M_{2,3}$ edges of 3*d*-transition metal elements.[1] We have performed diagnosis on the polarization for the beamline BL8B1 and characterization of the transmission multilayers with an elliptometric method.[1,2] This report is narrowed down to the performance of an Al/YB_6 37 layer film for use around 65 eV due to limitations of space. The monochromator was operated with the grating G3 and the mirror M22 used. The experimental setup is illustrated in fig. 1.

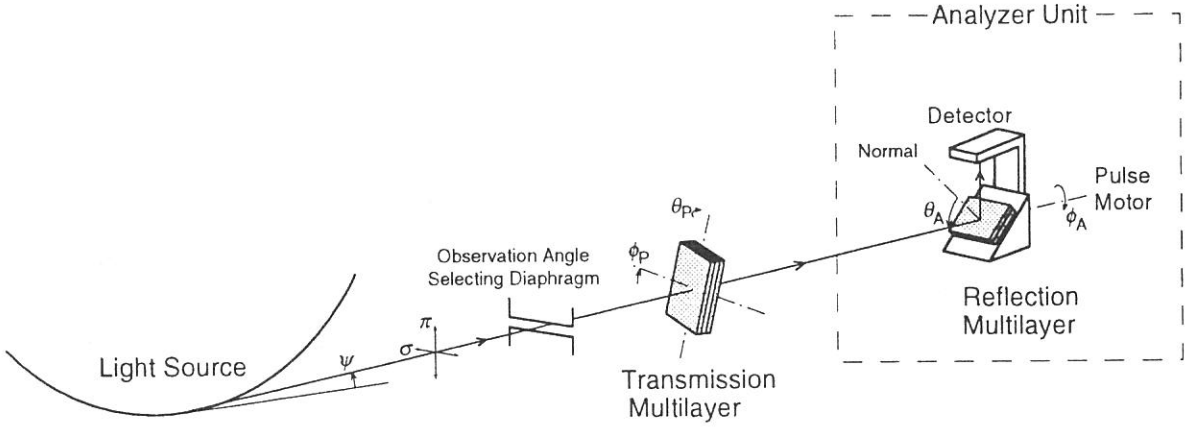

Fig. 1. Experimental setup at BL8B1.

Using an Al/YB_6 reflection multilayer as an analyzer, we made a preliminary investigation of the optics alignment of the beamline BL8B1 by studying the polarization property without a transmission multilayer.[2] The vertical aperture of the diaphragm just before the pre-mirror M1, was fixed at 1.5 mm and its middle level was positioned so that the lower end of M1 was irradiated to select the angle of observation ψ at ψ_1 as shown in fig. 2. In another configuration, the diaphragm was displaced to the position of $\psi = \psi_2$, where the upper end of M1 was irradiated. The displacement was 5.8 mm, which

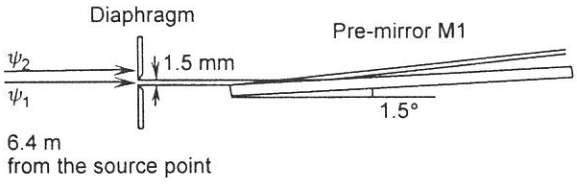

Fig. 2. Schematic of the observation angle selecting diaphragm in front of the pre-mirror M1.

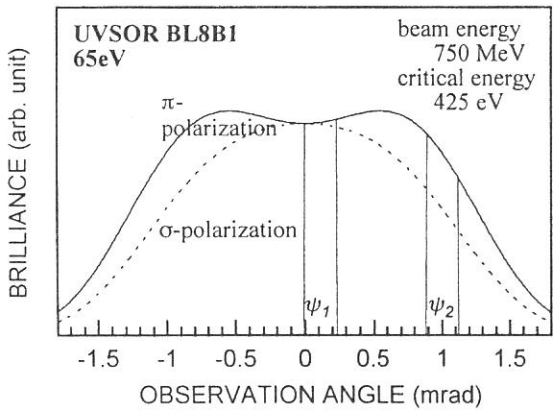

Fig. 3. Calculated intensity of σ- and π-components of BL8B1, UVSOR at the photon energy 65 eV as a function of the observation angle.

corresponds to $\psi_2 - \psi_1 = 0.9$ mrad. The state of polarization of the beam monochromatized at 65 eV was evaluated using so-called rotating analyzer unit, which gives the intensity ratio and the phase difference between σ- and π-components of bending radiation. Here we use $P_{SR} = (I_\sigma - I_\pi) / (I_\sigma + I_\pi)$ as a parameter to represent the degree of horizontal polarization. From the experimental results, P_{SR} was found to be 95% and 43% at $\psi = \psi_1$ and at $\psi = \psi_2$, respectively. Figure 3 illustrates the diaphragm position on the observation angle vs. brilliance curve calculated using the following parameters; the beam energy 750 MeV, the critical energy 425 eV and the photon energy 65 eV. It is noticed at BL8B1 that the angle for maximum intensity was observed between ψ_1 and ψ_2, which was not identical to $\psi = 0$. On the other hand, the phase difference δ_{SR} originally equals $\pm 90°$ depending on the sign of ψ, but will be retarded on the beamline optics by Δ_{BL}. Parameter values of $\delta_{SR} = 78.5°$ and $\Delta_{BL} = 11.5°$ were also obtained from the same measurements.

After the beamline diagnosis on the polarization, the Al/YB_6 transmission multilayer was inserted between the monochromator and the analyzer unit. The azimuthal angle ϕ_P was fixed at 0° and the angle of incidence θ_P was scanned from 38° to 50°. From the polarization measurements of transmitted light, the phase retardation $\Delta_P = \arg(t_s) - \arg(t_p)$ as well as the polarizance $P_P = (|t_p|^2 - |t_s|^2) / (|t_p|^2 + |t_s|^2)$ were analyzed using the values of P_{SR} and δ_{SR} evaluated in the preceding paragraph, where t_p and t_s are the amplitude transmission coefficients for p- and s-components, respectively. The experimental results are presented and compared with calculated ones as functions of the angle of incidence. The maximum polarizance and retardation were found to be 92% at $\theta_P = 42°$ and 68° at $\theta_P = 44°$, respectively.

One of the use of transmission multilayers is improvement of the degree of linear polarization as polarizers. When the source is linearly polarized to 95%, our polarizer of polarizance 92% can increase this to 99.8%, by which one can make precise measurements of optical rotation. Another use of transmission multilayers is generation of circular polarization as phase retarders. In the present case of $\Delta_P = -68°$ at $\theta_P = 44°$, linearly polarized light will be transformed into right- and left-handed 93% circular polarization by the retarder if the principal axis is oriented at $\phi_P = \pm 68°$.

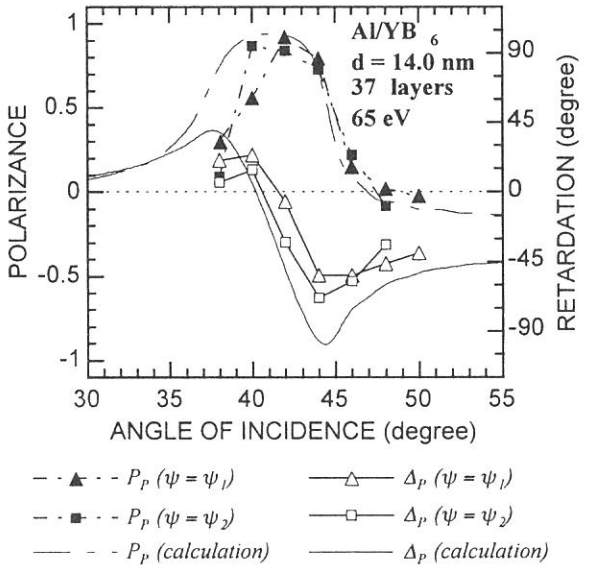

Fig. 4. Measured and calculated polarizances and retardations of the Al/YB_6 transmission multilayer as a function of angle of incidence at 65 eV. Polarizances measured at $\psi = \psi_1$ and $\psi = \psi_2$ are shown by closed triangles and squares, respectively, and retardations, by open triangles and squares.

REFERENCES

[1] W. Hu, T. Hatano, M. Yamamoto and M. Watanabe, J. Synch. Rad., (1998) (to be published).

[2] T. Hatano, W. Hu, M. Yamamoto and M. Watanabe, J. Electron Spectrosc. Relat. Phenom., (1998) (to be published).